(FAE) covers MALTs, and M cells in FAE are key antigen-sampling cells that present processed antigens to the APCs located below the M cells [6–8]. A ligand for FAE or M cells is a promising target molecule for mucosal vaccination. Claudin-4 was overexpressed in the FAE that covers GALTs and NALTs and in M cells [9–12]. These findings indicated that claudin-4-targeting is a promising strategy for mucosal vaccination.

Claudin, a tetra-transmembrane protein family with a molecular weight of ~23 kDa, comprises at least 27 family members [13,14]. Claudin-4 ligands show promise in the development of claudin-targeted mucosal vaccines; however, claudin-4 ligands, including antibodies, have never been fully developed because of low antigenicity and difficulty in preparing recombinant protein.

Clostridium perfringens enterotoxin (CPE) is a food poison in humans. Claudin-3 and -4 are receptors for CPE [15,16]. Interestingly, the C-terminal half of CPE binds to claudin-3 and -4 with no cytotoxicity [16,17]. This C-terminal fragment of CPE, which corresponds to amino acids 184–319 (C-CPE184), was the only known claudin binder prior to 2005. As such, it is the best characterized claudin binder. We previously found that C-CPE184 and the C-terminal fragment corresponding to amino acids 194–319, called C-CPE194, function as claudin-4-targeting ligands [18,19]. To investigate whether claudin-4-targeting could be a potent method for mucosal vaccination, we fused C-CPE184 with an experimental antigen and found that intranasal immunization of mice with the fusion protein activated antigen-specific mucosal and systemic immune responses and that these immune responses attenuated deletion of the claudin-4 binding domain. Thus, we demonstrated proof-of-concept that claudin-4 targeting may be a potent strategy for mucosal vaccination.

To develop a claudin binder with C-CPE184 as a prototype, we identified the functional residues of C-CPE184 by using serial deletion and site-directed mutagenesis. Substitution of certain residues with alanine increased binding to claudin-4, whereas deletion of the N-terminal 10 amino acids of C-CPE184 (C-CPE194) increased its solubility by over 30-fold over that of C-CPE184, with no change in affinity to claudin-4 [20–24]. Based on these findings, here, we prepared a fusion protein to serve as a model antigen containing a double alanine-substituted C-CPE194 mutant (Asn and Ser at position 309 and 313, respectively), and investigated mucosal vaccination by nasal immunization with the fused antigen.

2. Materials and methods

2.1. Preparation of C-CPEs and C-CPE-fused ovalbumin (OVA)

Fragments of alanine-substituted C-CPE194 were amplified by using polymerase chain reaction with C-CPE194 cDNAs as a template with appropriate primers for each mutant [23]. The resultant C-CPE fragments were cloned into the pET16b vector (Novagen, Darmstadt, Germany). Expression plasmids encoding fusion proteins of OVA with C-CPEs were prepared as follows: oligonucleotides containing the G4S linker and multi-cloning sites, including the KpnI, SpeI, SmaI, and PacI sites, were subcloned into NdeI-digested pET16b encoding C-CPEs, resulting in pET-MCS-C-CPEs. The OVA cDNA fragment was inserted into pET-MCS-C-CPEs at the KpnI/PacI site, resulting in pET-OVA-C-CPEs. The OVA-C-CPE-expression plasmids were transduced into *Escherichia coli* strain BL21 (DE3), and production of recombinant proteins was induced by the addition of isopropyl-D-thiogalactopyranoside. The harvested cells were lysed in buffer A (10 mM Tris–HCl, pH 8.0, 400 mM NaCl, 5 mM $MgCl_2$, 0.1 mM phenylmethylsulfonyl fluoride, 1 mM 2-mercaptoethanol, and 10% glycerol). The lysates were applied to HiTrap™ HP (GE Healthcare, Buckinghamshire, UK), and the OVA-C-CPE proteins were eluted with imidazole. The solvent was exchanged with phosphate-buffered saline (PBS) by using a PD-10 column (GE Healthcare), and the purified protein was stored at −80 °C until use. Purification of the recombinant proteins was confirmed by use of sodium dodecyl sulfate–polyacrylamide gel electrophoresis (SDS–PAGE), followed by staining with coomassie brilliant blue. A protein assay was carried out by using a BCA protein assay kit (Pierce Chemical, Rockford, IL) with bovine serum albumin as a standard.

2.2. Preparation of claudin-displaying budded baculovirus (BV)

Claudin-1 and -4 cDNAs were cloned into the baculoviral transfer vector pFastBac1 (Invitrogen, Gaithersburg, MD). Recombinant BVs were prepared by using the Bac-to-Bac system according to the manufacturer's protocols (Invitrogen). Briefly, Sf9 cells were infected with recombinant baculovirus. Seventy-two hours later, the BV fraction was isolated from the culture supernatant of the infected Sf9 cells by centrifugation. The pellets of the BV fraction were suspended in Tris-buffered saline (TBS) containing protease inhibitor cocktail (Sigma-Aldrich, St. Louis) and then stored at 4 °C. The claudin-displaying BVs were confirmed by use of SDS–PAGE and immunoblotting with anti-claudin antibodies.

2.3. Enzyme-linked immunosorbent assay (ELISA)

The claudin-displaying BVs were adsorbed onto wells in immunoplates (Nunc, Roskilde, Denmark). After well blocking with BlockAce (Dainippon Sumitomo Pharma, Osaka, Japan), OVA-C-CPEs were added to the wells and incubated. The wells were then washed with PBS and incubated with an anti-his-tag antibody, followed by incubation with a horseradish peroxidase-labeled secondary antibody. The immune-reactive proteins were detected by use of the TMB peroxidase substrate (Kirkegaard & Perry Laboratories, Inc., MD). Immuno-reactive proteins were measured at 450 nm.

2.4. Fluorescence activated cell sorting (FACS) analysis

L cells, claudin-1 or -4-expressing L cells (kindly provided by Dr. S. Tsukita, Kyoto University, Japan) were incubated with OVA-C-CPEs for 1 h at 4 °C, followed by incubation with an anti-his-tag antibody. Then, the cells were incubated with a fluorescein-labeled secondary antibody, and the OVA-C-CPE-bound cells were detected and analyzed with a flow cytometer (FACSCallibur, Becton Dickinson, NJ).

2.5. Animals

Female Balb/c mice and C57BL/6 mice (6–8-weeks-old) were purchased from SLC Inc. (Shizuoka, Japan). They were maintained in a room at 23 °C ± 1.5 °C with a 12-h light/dark cycle and were allowed free access to standard chow and water. After their arrival, the mice were maintained for at least 1 week to adapt to this environment before being used in the experiments. All animal experiments were performed according to the guidelines of Osaka University.

2.6. Nasal immunization

Balb/c mice were nasally immunized with OVA-C-CPEs once a week for three weeks at doses equivalent to 0.5, 1.0, or 5.0 μg of OVA. Seven days after the last immunization, serum and mucosal secretions (nasal washes, vaginal washes, and fecal extracts) were collected. Fecal pellets (100 mg) were suspended in 1 ml of PBS and extracted by vortexing for 10 min. The samples were centrifuged, and the resultant supernatants were used as fecal extracts. Nasal and vaginal mucosa were washed with 200 μl or 100 μl of PBS, respectively.

2.7. Production of an OVA-specific antibody

The titers of OVA-specific antibody in the serum, mucosal washes, and extracts were determined by using ELISA. Briefly, an immunoplate was coated with OVA (100 μg/well in a 96-well plate). Ten-fold serial dilutions of samples were added to the immunoplate and then reacted with horseradish peroxidase-conjugated anti-mouse IgG, IgG1, IgG2a, or IgA. The OVA-specific antibodies were detected by using the TMB peroxide substrate. End-point titers were expressed as the dilution ratio that gave 0.1 above the control values obtained from the serum of naïve mice at an absorbance of 450 nm.

2.8. Cytokine ELISA

Splenocytes were isolated from the spleens of immunized mice. After stimulation of the cells with vehicle or OVA, interferon-γ (IFN-γ) and interleukin-13 (IL-13) in the conditioned medium were measured with an ELISA kit according to the manufacturer's protocol (R&D Systems, Inc., MN).

2.9. Anti-tumor activity

C57BL/6 mice were nasally immunized with OVA-C-CPEs once a week for three weeks at a dose of 5 μg OVA. Seven days after the last immunization, a murine thymoma cell model EG7-OVA cells (1×10^6 cells) were subcutaneously inoculated into the mice. Tumor volumes were monitored and calculated by using the following equation: $a \times b \times b/2$, where "a" and "b" are the maximum and minimum diameters of the tumor, respectively.

3. Results

3.1. Preparation of OVA-C-CPEs

C-CPE184 was the only claudin-4 binder, and we previously proposed claudin-4-targeted mucosal absorption, cancer-targeting, and mucosal vaccination using C-CPE184 as a model for claudin-4 binding [9,16,18,25]. To improve the claudin-4-targeting system, we investigated the functional domain of C-CPE184 by preparing N-terminal and C-terminal truncated mutants, as well as alanine-substituted mutants. Substitution of Asn at position 309 or Ser at position 313 with Ala increased binding of C-CPE184 to claudin-4 [20]. Deletion of the N-terminal 10 amino acids in C-CPE184, to create C-CPE194 in this study, increased its solubility in PBS by 30-fold over that of C-CPE184 [24]. Given these results, we prepared double alanine-substituted C-CPE194 at positions 309 and 313 (C-CPE194$_{N309A/S313A}$) and found that C-CPE194$_{N309A/S313A}$ had higher affinity for claudin-4 than did C-CPE184 or C-CPE194 [22]. To investigate whether C-CPE194$_{N309A/S313A}$ could be used as a claudin-4-targeted mucosal vaccine, we prepared fusion proteins of the popular experimental antigen OVA with the C-CPEs (Fig. 1A–C). OVA-C-CPE303 served as a negative control, in which the claudin-4-binding domain was deleted [9,21].

To investigate the interaction of the OVA-C-CPEs with claudins, we performed an ELISA using claudin-displaying BV. OVA-C-CPE303 did not bind to wild-BV, claudin-1-displaying BV, or claudin-4-displaying BV (Fig. 2A). In contrast, OVA-C-CPE194 and OVA-C-CPE194$_{N309A/S313A}$ bound to claudin-4-displaying BV, but not to wild-BV or claudin-1-displaying BV. The double alanine-substituted mutant may, therefore, have a higher affinity than OVA-C-CPE194 for claudin-4 (Fig. 2A). To confirm the interaction of the OVA-C-CPEs with the claudins, we carried out FACS analysis with claudin-expressing cells. OVA-C-CPE194$_{N309A/S313A}$ specifically bound to claudin-4-expressing cells (Fig. 2B).

3.2. Mucosal vaccination using C-CPE mutants

Next, to evaluate mucosal vaccination with OVA-C-CPE194$_{N309A/S313A}$, mice were intranasally administered OVA-C-CPE194$_{N309A/S313A}$ once a week for three weeks. One week after the last immunization, we determined the serum OVA-specific IgG and OVA-specific IgA levels in nasal and vaginal washes, and fecal extracts. Administration of >0.5 μg of OVA-C-CPE194$_{N309A/S313A}$ markedly increased serum OVA-specific IgG compared to administration of OVA alone. Serum OVA-specific IgG levels were 11.2-fold higher in mice immunized with OVA-C-CPE194$_{N309A/S313A}$ than in mice immunized with OVA-C-CPE194 at a dose of 1.0 μg (Fig. 3A). Nasal, vaginal and fecal OVA-specific IgA levels were also increased in mice immunized with OVA-C-CPE194$_{N309A/S313A}$ 4.4-fold, 7.4-fold, >10-fold compared to those in mice immunized with OVA-C-CPE194, respectively (Fig. 3B–D).

Antigen-specific immune responses by mucosal vaccination are classified as Th1- and Th2-type responses [26,27]. Claudin-4-targeted antigen activates both Th1- and Th2-type immune responses [9]. To evaluate whether claudin-targeting using OVA-C-CPE194$_{N309A/S313A}$ also activates Th1- and Th2-type immune responses, we measured production of IgG1 (a Th2 response) and IgG2a (a Th1 response). OVA-specific IgG1 and IgG2a levels increased 165-fold and 27.0-fold,

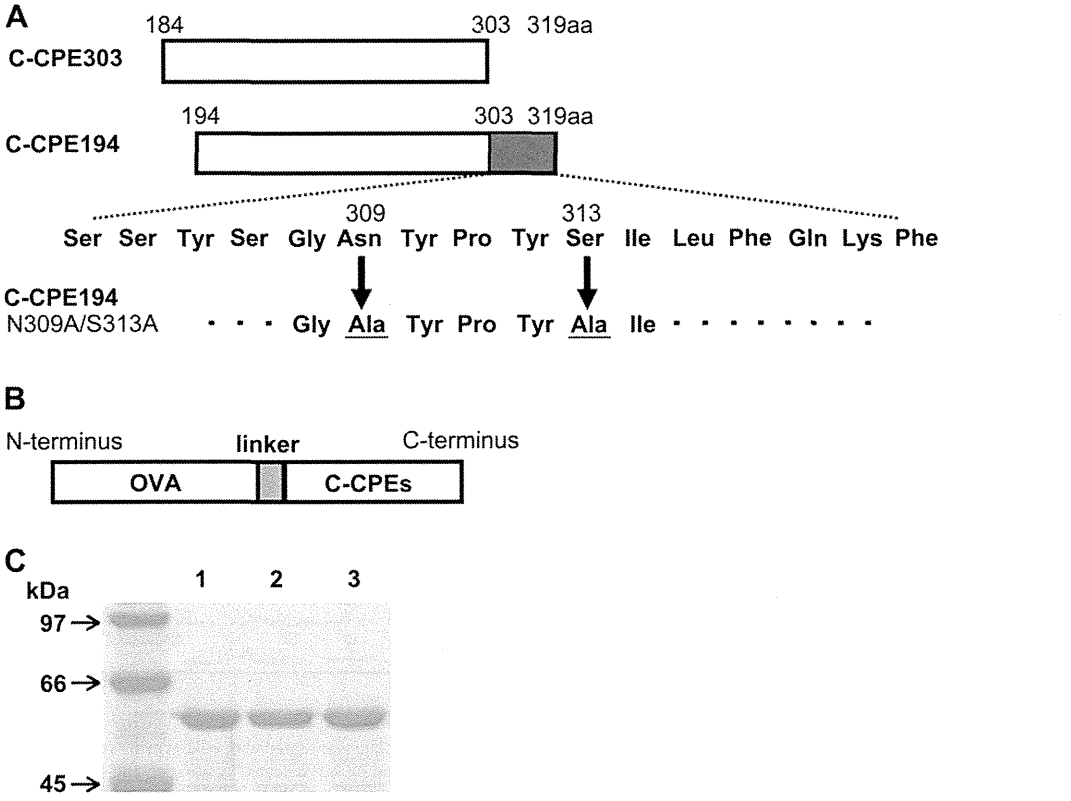

Fig. 1. Preparation of OVA-C-CPEs (A) Schematic illustration of C-CPEs. The C-terminal 16 amino acid-fragment contains the claudin-4 binding domains [21]; site-directed mutagenesis revealed that substitution of Asn at position 309 and Ser at position 313 with alanine increases claudin-4 binding [20]. C-CPE194 is the C-terminal fragment of CPE that corresponds to amino acids 194–319 [23]. (B) Schematic drawing of OVA-C-CPEs. OVA was linked with C-CPE303, C-CPE194, or C-CPE194$_{N309A/S313A}$ via a linker as described in the Materials and Methods. (C) Preparation of OVA-C-CPEs. OVA-C-CPEs were subjected to SDS–PAGE, followed by staining with coomassie brilliant blue. Lane 1, OVA-C-CPE303 (62 kDa); lane 2, OVA-C-CPE194 (62 kDa); lane 3, OVA-C-CPE194$_{N309A/S313A}$ (62 kDa). (For interpretation of the references to colour in this figure legend, the reader is referred to the web version of this article.)

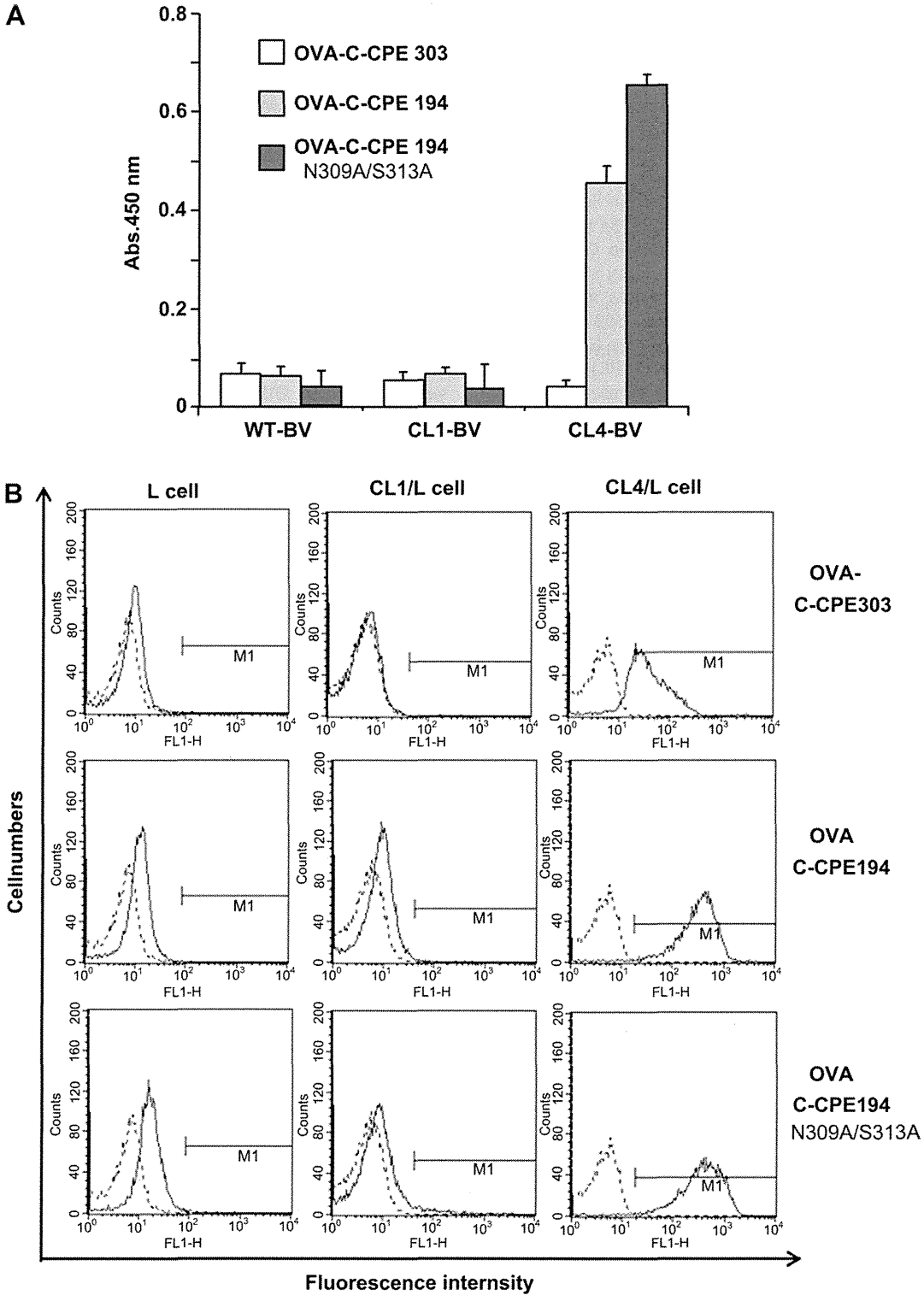

Fig. 2. Interaction of OVA-C-CPEs with claudin-4. (A) ELISA using claudin-displaying BV. An immunoplate was coated with wild-type BV (WT-BV), claudin-1-displaying BV (CL1-BV) or claudin-4-displaying BV (CL4-BV). Vehicle or OVA-C-CPE was added to each well. OVA-C-CPE-bound BV was detected by using an anti-his tag antibody and a peroxidase-labeled antibody as described in the Materials and Methods. Data are means ± SD ($n = 4$) and are representative of three independent experiments. (B) FACS analysis using claudin-expressing cells. L, claudin-1-expressing L cells (CL1/L cells) or claudin-4-expressing L cells (CL4/L cells) were treated with OVA-C-CPEs. Then, OVA-C-CPE-bound cells were detected by using an anti-his tag antibody followed by a fluorescein-labeled secondary antibody. Labeled cells were detected by use of FACS. The dotted line represents the histograms of the background in the absence of the primary antibody. The solid line indicates the histograms of the OVA-C-CPE-bound cells. Data are representative of three independent experiments.

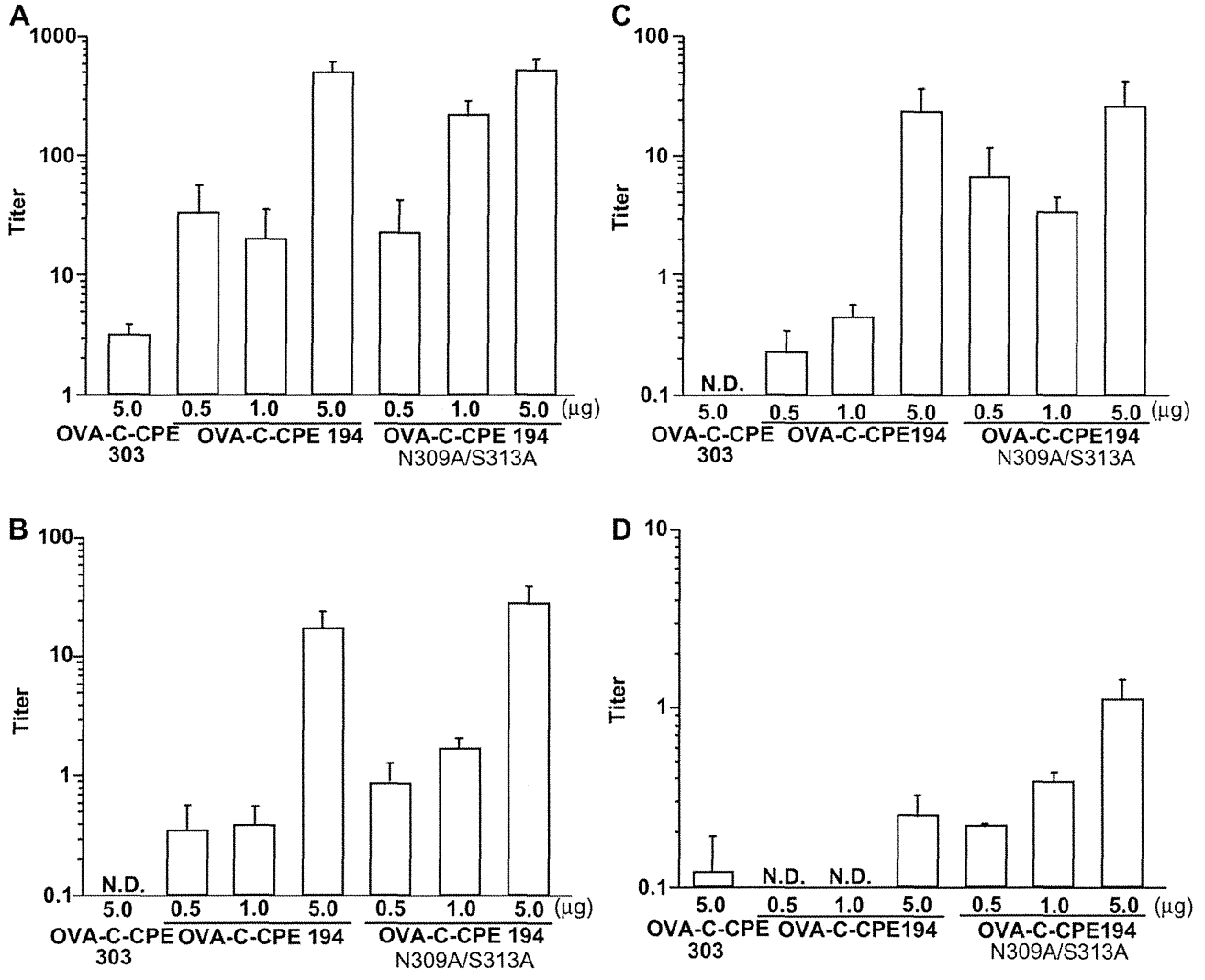

Fig. 3. Production of OVA-specific antibodies by nasal immunization with OVA-C-CPEs. Mice were nasally immunized with C-CPEs-fused OVA once a week for three weeks at the indicated doses. One week after the last immunization, serum, mucosal washes, and fecal extracts were recovered. OVA-specific serum IgG (A), nasal IgA (B), vaginal IgA (C) and fecal IgA (D) levels were measured as described in the Materials and Methods. Data are means ± SEM ($n = 4$).

respectively, in mice immunized with OVA-C-CPE194$_{N309A/S313A}$ compared to mice immunized with OVA-C-CPE194 (1 μg of OVA), respectively (Fig. 4A). Th1-specific (IFN-γ) and Th2- specific (IL-13) cytokines in splenocytes isolated from mice nasally immunized with OVA-C-CPE194$_{N309A/S313A}$ also increased 1.7-fold and 3.1-fold, respectively, relative to those from mice immunized with OVA-C-CPE194 (Fig. 4B).

Finally, we investigated the effect of mucosal vaccination on an experimental tumor model by using OVA-expressing cancer cells. Nasal immunization of mice with OVA or OVA-C-CPE303 did not suppress tumor growth (3044 ± 351 mm^3 in vehicle; 2250 ± 470 mm^3 in OVA; 3254 ± 573 mm^3 in OVA-C-CPE303 on day 24); however, immunization with OVA-C-CPE194 or OVA-C-CPE194$_{N309A/S313A}$ did suppress tumor growth (1143 ± 511 mm^3 and 399 ± 163 mm^3 on day 24, respectively). The double-alanine substituted mutant showed higher anti-tumor activity than that of OVA-C-CPE194 (Fig. 5). These results indicate that C-CPE194$_{N309A/S313A}$ may be a potent claudin ligand for mucosal vaccination.

4. Discussion

Efficient delivery of antigen to MALTs is pivotal for mucosal vaccination. Claudin-4 was expressed in FAE covering MALTs, and claudin-4-targeting has been proposed as a strategy for the development of mucosal vaccines [9,12]. The extracellular domain of claudin is weakly antigenic, and preparation of claudin proteins is difficult because of their hydrophobicity. Accordingly, the development of claudin-4 ligands has been limited. Here, we focused on C-CPE, which is the first identified claudin binder and found that the double alanine-substituted C-CPE194$_{N309A/S313A}$ can serve as a potent claudin ligand for the development of mucosal vaccination.

Efficient delivery of antigen to MALTs, which contain lymphocytes, M cells, T cells, B cells, and APCs, is an essential component of mucosal vaccine effectiveness [2]. Claudin-4 was expressed on FAE covering MALTs [9,12]. Lymphocytes, T cells, and B cells localize below the FAE [7,8]. FAE forms epithelial cell sheets that cover MALTs, and modulation of the TJ-seal in FAE can cause the influx of antigens to the immune-potent cells beneath the FAE. The claudin-4 binder disrupts the mucosal TJ-barrier [25]. C-CPE194$_{N309A/S313A}$ is a more potent modulator of the TJ-barrier than is C-CPE194 [22]. One possible explanation for the effectiveness of mucosal vaccination with C-CPE194$_{N309A/S313A}$ may be the influx of antigen into the immune-potent cells by modulation of the TJ-seal in the FAE. A mixture of C-CPE184 and OVA did not activate OVA-specific immune responses, whereas C-CPE184-fused OVA did. The targeting of antigen to claudin-4 is essential for mucosal vaccination

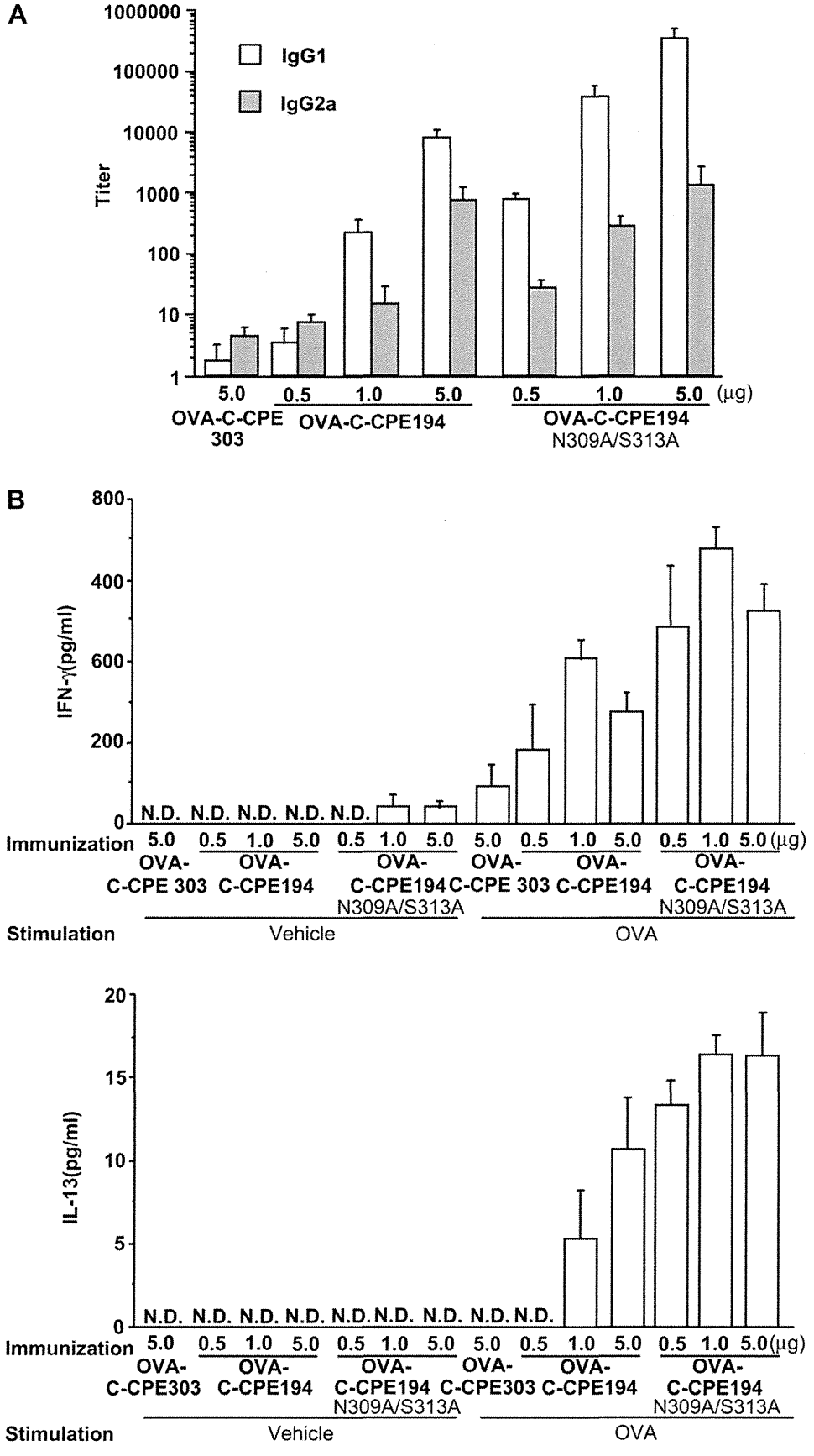

Fig. 4. Activation of Th1- and Th2-type immune responses by nasal immunization with OVA-C-CPEs. Mice were nasally immunized with C-CPEs-fused OVA once a week for three weeks at the indicated doses. One week after the last immunization, serum and splenocytes were recovered. OVA-specific serum IgG1 and IgG2a levels were measured as described in the Materials and Methods (A). The splenocytes were stimulated with OVA (1 mg/ml), and IFN-γ and IL-13 levels in the conditioned medium were measured by using a commercially available kit according to the manufacture's protocols (B). Data are means ± SEM ($n = 4$). The results are representative of three independent experiments.

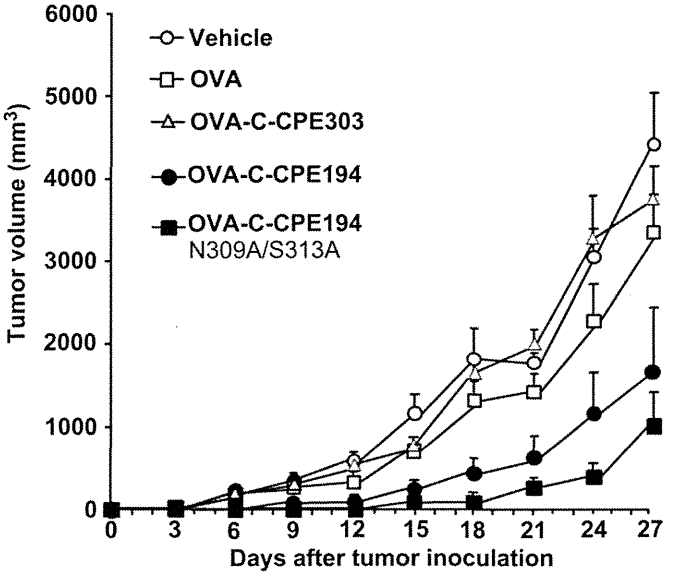

Fig. 5. Anti-tumor activity following immunization with OVA-C-CPE194$_{N309A/S313A}$. C57BL/6 mice were nasally immunized with vehicle, OVA, OVA-C-CPE303, OVA-C-CPE194, or OVA-C-CPE194$_{N309A/S313A}$ (5 μg of OVA) once a week for three weeks. Seven days after the last immunization, the mice were subcutaneously injected on the right back with 1×10^6 EG7-OVA cells. Tumor growth was monitored by measuring two diameters, and tumor volumes were calculated by using the following equation: $a \times b \times b/2$, where "a" is the maximum diameter of the tumor and "b" is the minimum diameter of the tumor. Data are means ± SEM ($n = 5$). The results are representative of two independent experiments.

using the claudin-4 binder [9], but the possibility of this may be negligible.

M cells are specialized antigen-sampling epithelial cells, beneath which various immune cells are localized. M cells deliver antigens from the lumen to the intraepithelial lymphoid cells via active transepithelial transport [6,28,29]. Rajapaksa et al. showed that claudin-4-targeted particles coated with the claudin-4-binding peptide are taken up by M cells, suggesting that claudin-4 is expressed on M cells [30]. Claudin-4 contains a clathrin-sorting signal in its intracellular C-terminal domain, and the claudin-4-targeting molecule is taken up by clathrin-mediated endocytosis [31]. The C-CPE194$_{N309A/S313A}$-fused antigen may be delivered more efficiently to M cells than the C-CPE194-fused antigen, followed by efficient delivery of antigen to the intraepithelial lymphoid cells. The association constant of C-CPE194$_{N309A/S313A}$ is 6.67×10^5 Ms^{-1}, which is similar to that of C-CPE194 (7.13×10^5 Ms^{-1}). In contrast, the dissociation constant of C-CPE194$_{N309A/S313A}$ is 3.05×10^{-5} S^{-1}, which is smaller than that of C-CPE194 (3.24×10^{-4} S^{-1}) [22]. C-CPE194$_{N309A/S313A}$-fused OVA might interact with claudin-4 longer than C-CPE194-fused OVA, resulting in efficient uptake of OVA into M cells. Claudin-4-targeting mucosal vaccination might be activated by uptake of antigen into M cells. Further analyses of the affinity of the fusion protein for claudin-4 and of the cellular uptake of the fusion protein are needed to clarify the mode of action.

Importantly, the claudin-4-targeting system activated immune responses without any adjuvant. Combining the claudin-4-targeting system with vaccine adjuvant may, therefore, create an even more effective mucosal vaccine. Antibodies are popular ligands for membrane proteins; however, the establishment of an anti-claudin antibody had been problematic because of its low antigenicity. Commercially available antibodies for claudin recognize the intracellular domain of claudins. Recently, two groups successfully prepared antibodies against the extracellular loop domain of claudin. Suzuki et al. immunized mice that had an autoimmune disease with claudin-4-expressing cells and raised an anti-claudin-4 antibody [32]. Fofana et al. immunized a rat with a DNA vector encoding claudin-1 to prepare an anti-claudin-1 antibody [33]. Soon, a claudin-targeted mucosal vaccine based on C-CPE mutants and/or antibodies will be developed.

5. Conclusions

We found that C-CPE194$_{N309A/S313A}$ worked as a potent claudin-4 ligand for the development of a mucosal vaccine. We could reduce the administered dose of the antigen using C-CPE194$_{N309A/S313A}$ more than C-CPE184 or C-CPE194, leading to reduction of the costs and the risk of anaphylaxis. Claudins have been considered as targets for mucosal vaccines, cancer therapy, and non-invasive drug absorption. The C-CPE mutant evaluated in this study shows promise as a lead claudin-4 ligand for claudin-targeted drug development.

Acknowledgments

We thank Drs Y. Horiguchi (Osaka University) and M. Furuse (Kobe University) for providing us with the C-CPE cDNA and claudin cDNA, respectively. This work was supported by a Grant-in-Aid for Scientific Research from the Ministry of Education, Culture, Sports, Science and Technology, Japan (21689006), by a Health and Labor Sciences Research Grant from the Ministry of Health, Labor and Welfare of Japan and by a grant from the Kansai Biomedical Cluster project in Saito, which is promoted by the Knowledge Cluster Initiative of the Ministry of Education, Culture, Sports, Science and Technology, Japan. H.S. is supported by Research Fellowships of the Japan Society for the Promotion of Science for Young Scientists.

References

[1] Jepson MA, Clark MA, Hirst BH. M cell targeting by lectins: a strategy for mucosal vaccination and drug delivery. Adv Drug Deliv Rev 2004;56:511–25.
[2] Kunisawa J, Nochi T, Kiyono H. Immunological commonalities and distinctions between airway and digestive immunity. Trends Immunol 2008;29:505–13.
[3] O'Hagan DT, Singh M. Microparticles as vaccine adjuvants and delivery systems. Expert Rev Vaccines 2003;2:269–83.
[4] Ryan EJ, Daly LM, Mills KH. Immunomodulators and delivery systems for vaccination by mucosal routes. Trends Biotechnol 2001;19:293–304.
[5] Vogel K, Kantor J, Wood L, Rivera R, Schlom J. Oral immunization with enterocoated microbeads induces antigen-specific cytolytic T-cell responses. Cell Immunol 1998;190:61–7.
[6] Neutra MR, Frey A, Kraehenbuhl JP. Epithelial M cells: gateways for mucosal infection and immunization. Cell 1996;86:345–8.
[7] Owen RL. Sequential uptake of horseradish peroxidase by lymphoid follicle epithelium of Peyer's patches in the normal unobstructed mouse intestine: an ultrastructural study. Gastroenterology 1977;72:440–51.
[8] Owen RL, Piazza AJ, Ermak TH. Ultrastructural and cytoarchitectural features of lymphoreticular organs in the colon and rectum of adult BALB/c mice. Am J Anat 1991;190:10–8.
[9] Kakutani H, Kondoh M, Fukasaka M, Suzuki H, Hamakubo T, Yagi K. Mucosal vaccination using claudin-4-targeting. Biomaterials 2010;31:5463–71.
[10] Kuo WL, Lee LY, Wu CM, Wang CC, Yu JS, Liang Y, et al. Differential expression of claudin-4 between intestinal and diffuse-type gastric cancer. Oncol Rep 2006;16:729–34.
[11] Ling J, Liao H, Clark R, Wong MS, Lo DD. Structural constraints for the binding of short peptides to claudin-4 revealed by surface plasmon resonance. J Biol Chem 2008;283:30585–95.
[12] Tamagawa H, Takahashi I, Furuse M, Yoshitake-Kitano Y, Tsukita S, Ito T, et al. Characteristics of claudin expression in follicle-associated epithelium of Peyer's patches: preferential localization of claudin-4 at the apex of the dome region. Lab Invest 2003;83:1045–53.
[13] Furuse M, Tsukita S. Claudins in occluding junctions of humans and flies. Trends Cell Biol 2006;16:181–8.
[14] Mineta K, Yamamoto Y, Yamazaki Y, Tanaka H, Tada Y, Saito K, et al. Predicted expansion of the claudin multigene family. FEBS Lett 2011;585:606–12.
[15] Morita K, Furuse M, Fujimoto K, Tsukita S. Claudin multigene family encoding four-transmembrane domain protein components of tight junction strands. Proc Natl Acad Sci U S A 1999;96:511–6.
[16] Sonoda N, Furuse M, Sasaki H, Yonemura S, Katahira J, Horiguchi Y, et al. *Clostridium perfringens* enterotoxin fragment removes specific claudins from tight junction strands: evidence for direct involvement of claudins in tight junction barrier. J Cell Biol 1999;147:195–204.

[17] Katahira J, Inoue N, Horiguchi Y, Matsuda M, Sugimoto N. Molecular cloning and functional characterization of the receptor for *Clostridium perfringens* enterotoxin. J Cell Biol 1997;136:1239–47.
[18] Ebihara C, Kondoh M, Hasuike N, Harada M, Mizuguchi H, Horiguchi Y, et al. Preparation of a claudin-targeting molecule using a C-terminal fragment of *Clostridium perfringens* enterotoxin. J Pharmacol Exp Ther 2006;316:255–60.
[19] Saeki R, Kondoh M, Kakutani H, Tsunoda SI, Mochizuki Y, Hamakubo T, et al. A novel tumor-targeted therapy using a claudin-4-targeting molecule. Mol Pharmacol 2009;76:918–26.
[20] Takahashi A, Komiya E, Kakutani H, Yoshida T, Fujii M, Horiguchi Y, et al. Domain mapping of a claudin-4 modulator, the C-terminal region of C-terminal fragment of *Clostridium perfringens* enterotoxin, by site-directed mutagenesis. Biochem Pharmacol 2008;75:1639–48.
[21] Takahashi A, Kondoh M, Masuyama A, Fujii M, Mizuguchi H, Horiguchi Y, et al. Role of C-terminal regions of the C-terminal fragment of *Clostridium perfringens* enterotoxin in its interaction with claudin-4. J Control Release 2005; 108:56–62.
[22] Takahashi A, Kondoh M, Uchida H, Kakamu Y, Hamakubo T, Yagi K. Mutated C-terminal fragments of *Clostridium perfringens* enterotoxin have increased affinity to claudin-4 and reversibly modulate tight junctions in vitro. Biochem Biophys Res Commun 2011;410:466–70.
[23] Uchida H, Kondoh M, Hanada T, Takahashi A, Hamakubo T, Yagi K. A claudin-4 modulator enhances the mucosal absorption of a biologically active peptide. Biochem Pharmacol 2010;79:1437–44.
[24] Van Itallie CM, Betts L, Smedley 3rd JG, McClane BA, Anderson JM. Structure of the claudin-binding domain of *Clostridium perfringens* enterotoxin. J Biol Chem 2008;283:268–74.
[25] Kondoh M, Masuyama A, Takahashi A, Asano N, Mizuguchi H, Koizumi N, et al. A novel strategy for the enhancement of drug absorption using a claudin modulator. Mol Pharmacol 2005;67:749–56.
[26] Yamamoto S, Kiyono H, Yamamoto M, Imaoka K, Fujihashi K, Van Ginkel FW, et al. A nontoxic mutant of cholera toxin elicits Th2-type responses for enhanced mucosal immunity. Proc Natl Acad Sci U S A 1997;94:5267–72.
[27] Yanagita M, Hiroi T, Kitagaki N, Hamada S, Ito HO, Shimauchi H, et al. Nasopharyngeal-associated lymphoreticular tissue (NALT) immunity: fimbriae-specific Th1 and Th2 cell-regulated IgA responses for the inhibition of bacterial attachment to epithelial cells and subsequent inflammatory cytokine production. J Immunol 1999;162:3559–65.
[28] Kraehenbuhl JP, Neutra MR. Molecular and cellular basis of immune protection of mucosal surfaces. Physiol Rev 1992;72:853–79.
[29] Yuki Y, Kiyono H. New generation of mucosal adjuvants for the induction of protective immunity. Rev Med Virol 2003;13:293–310.
[30] Rajapaksa TE, Stover-Hamer M, Fernandez X, Eckelhoefer HA, Lo DD. Claudin 4-targeted protein incorporated into PLGA nanoparticles can mediate M cell targeted delivery. J Control Release 2010;142:196–205.
[31] Ivanov AI, Nusrat A, Parkos CA. Endocytosis of epithelial apical junctional proteins by a clathrin-mediated pathway into a unique storage compartment. Mol Biol Cell 2004;15:176–88.
[32] Suzuki M, Kato-Nakano M, Kawamoto S, Furuya A, Abe Y, Misaka H, et al. Therapeutic antitumor efficacy of monoclonal antibody against Claudin-4 for pancreatic and ovarian cancers. Cancer Sci 2009;100:1623–30.
[33] Fofana I, Krieger SE, Grunert F, Glauben S, Xiao F, Fafi-Kremer S, et al. Monoclonal anti-claudin 1 antibodies prevent hepatitis C virus infection of primary human hepatocytes. Gastroenterology 2010;139:953–64.

World Journal of Clinical Oncology

Online Submissions: http://www.wjgnet.com/esps/
wjco@wjgnet.com
doi:10.5306/wjco.v3.i12.150

World J Clin Oncol 2012 December 10; 3(12): 150-154
ISSN 2218-4333 (online)

EDITORIAL

Multiple roles of angiotensin in colorectal cancer

Hiroki Kuniyasu

Hiroki Kuniyasu, Department of Molecular Pathology, Nara Medical University, 840 Shijo-cho, Kashihara 634-8521, Japan
Author contributions: Kuniyasu H contributed solely to this work.
Supported by Grant-in-Aid for Scientific Research from Japan Society for the Promotion of Science, Japan
Correspondence to: Hiroki Kuniyasu, MD, PhD, Professor, Chairman, Department of Molecular Pathology, Nara Medical University, 840 Shijo-cho, Kashihara 634-8521, Japan. cooninh@zb4.so-net.ne.jp
Telephone: +81-744-223051 Fax: +81-744-257308
Received: July 19, 2012 Revised: September 28, 2012
Accepted: November 17, 2012
Published online: December 10, 2012

Abstract

Colorectal cancer (CRC) cells express renin and chymase through which they can activate angiotensin. Renin expression is induced by hyperglycemic conditions. As angiotensinogen is produced in the liver, CRC cells that can activate angiotensin have an enhanced ability to metastasize to this organ. In human CRC cases, patients with diabetes have higher activities of rennin and angiotensin-II in primary tumors, and on average, have a more progressed disease stage, especially with respect to liver metastasis. These patients exhibit a stronger association with Hemoglobin A1c levels and metastasis compared to patients without diabetes. In a combined diabetes/CRC liver metastasis mouse model, concurrent treatment with anti-angiotensin and hypoglycemic agents shows a synergic effect in terms of reduced liver metastasis and improved survival. The effect of anti-angiotensin treatment and blood sugar control as a baseline management for colon cancer patients with diabetes needs to be examined in clinical trials to establish whether it can prevent liver metastasis.

Key words: Angiotensin; Renin; Angiotensin II receptor blocker; Diabetes; Liver metastasis

Peer reviewers: Antonio Araujo, MD, PhD, Medical Oncology Department, Portuguese Institute of Oncology – Porto Centre, R Dr Antonio Bernardino Almeida, 4200 Porto, Portugal; Bin Wu, MD, PhD, Professor and Chairman, Department of Gastroenterology and Endoscopy, The Third Affiliated Hospital, Sun Yat-sen University, China

Kuniyasu H. Multiple roles of angiotensin in colorectal cancer. *World J Clin Oncol* 2012; 3(12): 150-154 Available from: URL: http://www.wjgnet.com/2218-4333/full/v3/i12/150.htm DOI: http://dx.doi.org/10.5306/wjco.v3.i12.150

INTRODUCTION

Various factors participate in colorectal cancer (CRC) progression, such as growth factors, angiogenic factors, and cytokines. Angiotensin is a well-known hypertensive hormone and also possesses protumoral functions. Angiotensin II (A-II), an active form of angiotensin, induces angiogenesis, cell growth, invasion via activation of the specific receptor, A-II type 1 receptor (ATR1) to enhance development and progression of CRC. Some colorectal cancer cells possess the angiotensin-activating mechanism employing renin and chymase. Importantly, renin expression is upregulated by hyperglycemic condition. The data examining the importance of hyperglycemia/diabetes-induced angiotensin activation in the liver metastasis of colorectal cancer are described in this article.

PROTUMORAL EFFECT OF ANGIOTENSIN

Colorectal cancer is the fourth leading cause of cancer-related deaths in Japan, and cancer mortality continues to increase as the Western lifestyle gains popularity among the Japanese population[1]. Approximately 24% of CRC cases involving invasion beyond the submucosal layer showed liver metastasis during and/or after the operation to excise the tumor[2]. One-third of CRC patients died of liver metastasis[3], and only one-third or fewer CRC patients with liver metastasis respond to systemic chemotherapy, although even in these cases long-term

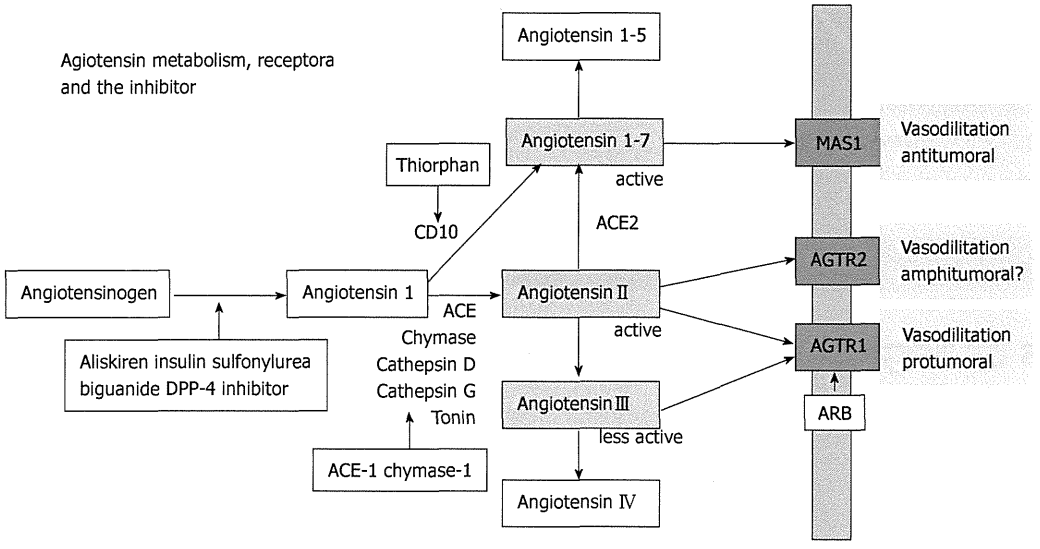

Figure 1

survival was rare[3]. The 5-year survival rate of CRC patients with liver metastasis is reported to be less than 20%[1]. The early detection and control of liver metastasis is therefore an important goal for the successful treatment of CRCs.

A-II has multiple physiological effects mediated by the activation of the ATR1. These include vasoconstriction, inflammation, and proliferation in cardiovascular and neoplastic tissues[4]. ATR1 intracellular signaling pathways produce diverse effects, including activation of protein kinase C, angiopoietin 2, vascular endothelial growth factor (VEGF), VEGF receptors, fibroblast growth factor, platelet-derived growth factor, transforming growth factor-beta, epidermal growth factor, nitric oxide synthase, and metalloproteinase[4,5]. These properties enhance colon carcinogenesis and disease progression.

We have experimentally confirmed the protumor effect of angiotensin by studying the effects of A-II on cell growth, invasion, and apoptosis in several CRC-derived cell lines[6]. A-II enhances cell growth and *in vitro* invasion into type IV collagen and reduces apoptosis in a dose-dependent manner. Reduction in hepatic angiotensinogen (ATG) production by knockdown with cholesterol-conjugated antisense S-oligodeoxynucleotide (S-ODN) suppressed liver metastasis of HT29 cells in a nude mouse liver metastasis model. ATG-knockdown mice had fewer and smaller metastatic foci with a lower Ki-67 labeling index and reduced microvessel density, compared to the control mice. Knockdown of renin or chymase in HT29 cells also resulted in smaller and fewer metastatic foci in the liver compared to the control. Furthermore, examination of 121 CRC patients showed that the serum A-II concentration is significantly associated with advanced disease stage, especially liver metastasis.

ANGIOTENSIN ACTIVATION IN CRC CELLS

As described above, the ability of angiotensin activation might be a prominent feature of cancer cell to obtain the powerful tool for progression. The mechanism of angiotensin activation in cancer is examined using colorectal cancer cell lines[6]. ATG is an inactive precursor of A-II (Figure 1), and has no effect on cancer cells prior to conversion to A-II. Effects of ATG on cell growth, invasion, and apoptosis were examined in HT29 cells. Interestingly, ATG enhanced cell growth, in vitro invasion, and anti-apoptotic survival in HT29 cells in a dose-dependent manner in a similar fashion to A-II. This finding suggests that the HT29 cells have an endogenous angiotensin-activating mechanism.

We then examined the expression of angiotensin-associated genes in HT29 cells[6]. They express ATR1, but not ATG or angiotensin I (A-I)-converting enzyme (ACE). However, they express chymase, which possesses an ACE-like activity. Renin is also expressed in HT29 cells, and a renin inhibitor abrogates the production of both A-I and A-II. A chymase inhibitor suppresses the production of A-II but not that of A-I. In contrast, an ACE inhibitor does not affect the production of A-I or A-II in HT29 cells. Thus, A-II is produced from ATG by renin and chymase in HT29 cells. Chymase, tonin, and cathepsin G all possess an ACE-like activity, which can be used as a substitute for ACE (Figure 1)[7]. Cathepsin D is responsible for producing A-I from ATG in cardiac myocytes, fibroblasts, and vascular smooth muscle cells in place of renin[8]. However, the CRC cells in this study did not express cathepsin D. Chymase expression is associated with hypoxia or ischemia in the human left cardiac ventricle[9]; it is not associated with hyperglycemia in CRC cells[6].

MAS1

MAS1 is a receptor of an A-II derivative produced by ACE 2-angiotensin 1-7 (A1-7), and has similar physiological effects to anti-A-II, including vessel dilation and reduction of blood pressure (Figure 1)[10]. We examined the role of

MAS1 in CRC and in invasive ductal carcinoma (IDC) of the breast[11]. MAS1 was not detected by immunohistochemistry in either CRCs or the normal colon mucosa. In contrast, normal mammary lobules and ducts expressed MAS1 at high levels, although MAS1 expression was attenuated in all IDCs. Of particular note was the greatly reduced MAS1 expression in scirrhous-type IDCs compared to other types. The decrease in MAS1 expression was associated with lymph node metastasis but not T factor, grade, or the status of the estrogen or progesterone receptor. The decrease in MAS1 expression was inversely associated with HER2 expression. Using a mouse breast cancer cell line, BALB-MC, which expresses MAS1, cell growth and in vitro invasion were examined. A1-7 treatment inhibited growth and invasion of BALB-MC cells, which were abrogated by MAS1 knockdown. MAS1 intracellular signaling involves Akt phosphorylation, protein kinase C activation, and mitogen-activated protein kinase inhibition[12]. These findings suggest that MAS1 might act as an inhibitory regulator of both normal breast tissue and breast cancer.

CD10

CD10, also known as common acute lymphoblastic leukemia antigen (CALLA), is a characteristic marker of various subgroups of B-cell type acute lymphocytic leukemia[13,14]. It is a zinc-dependent membrane metalloendopeptidase (also referred to as neutral endopeptidase (EC 3.4.24.11), enkephalinase, or neprilysin)[14]. CD10 is expressed in CRC and is associated with CRC metastases, especially liver metastasis[2,15,16]. Met-enkephalin (MENK) is a high-affinity substrate of CD10[17,18]. It is produced by hepatocytes under conditions of cellular stress, such as hepatitis, bile stasis, and liver metastasis[19-21]. MENK inhibits tumor growth and the establishment of metastatic foci[22]. CD10-positive CRC cells degrade MENK and escape from MENK-induced tumor suppression[22]. CD10 possesses a weak affinity to A-I [23]; however, CD10 shows A-I -degrading activity but not the A-I -converting activity. The degradation of A-I produces A1-7, a MAS1 ligand. As discussed above, MAS1 is not expressed in CRCs. CD10-induced A1-7 does not affect CRC progression.

DIABETES AND THE RENIN/ANGIOTENSIN SYSTEM

Diabetes mellitus is a common problem in countries adopting the Western lifestyle. Several epidemiological studies have shown an association between type 2 diabetes and the risk of colorectal, pancreatic, breast, liver, gastric, and endometrial cancer[24]. The risk of malignancies is increased at earlier stages in cases of abnormalities in glucose metabolism, and there is a linear relationship between cancer risk and plasma insulin levels[24]. With regard to CRCs, a meta-analysis of 15 studies, involving a total of 2 593 935 participants, showed that diabetes is associated with an increased risk of CRC [relative risk, 1.30; 95% confidence interval (CI), 1.20-1.40]. Diabetes is also associated with CRC mortality (relative risk, 1.26; 95% CI, 1.05-1.50)[25]. High glycated hemoglobin (HbA1c) levels are also associated with an increased risk of CRC (odds ratio, 1.57; 95% CI, 0.94-2.60)[26]. Several studies have demonstrated that hyperinsulinemia, elevated levels of C-peptide, elevated body mass index, high levels of insulin growth factor-1, low levels of insulin growth factor binding protein-3, high leptin levels, and low adiponectin levels are involved in carcinogenesis[27]. Increased blood concentrations of insulin and insulin-like growth factor are particularly important in enhancing the risk of CRC[28]. However, a detailed understanding of how diabetes might increase the risk of CRC is still lacking.

We examined the expression of renin in HT29 and CT26 cells in association with changing glucose concentration. When the medium contained 100 mg/dL glucose, renin protein was detected in HT29 cells but not in CT26 cells. When the medium contained glucose at 200 mg/dL or more, the expression of renin increased with increasing glucose concentration in a dose-dependent manner in both cell lines. CT26 cells also expressed chymase but not ACE, in a similar manner to HT29 cells. These findings suggest then that the CRC cells activate angiotensin when exposed to high glucose concentrations.

In the hyperglycemic mice fed with a high-glucose diet, the size, number, Ki67 labeling index, and microvessel density of the liver metastatic foci were greater than those in the normoglycemic mice fed with the control diet. Clinical studies have suggested that a similar situation exists in patients. In the examination of 121 CRC patients, the tumor renin concentration correlated with HbA1c levels and the tumor A-II concentration correlated with the tumor renin concentration. Moreover, high blood HbA1c levels are associated with a higher incidence of liver metastasis in diabetes cases but not non-diabetes cases. In cardiac fibroblasts, a high concentration of glucose significantly increases intracellular A-II levels by increasing the intracellular levels of renin[29].

A-II AND LIVER METASTASIS OF COLORECTAL CANCER

The A-II precursor, ATG is mainly produced in hepatocytes[30]. We confirmed that CRC cells possessing angiotensin-activating ability establish liver metastasis because they can produce abundant A-II from AGT in the liver[6]. To examine the prometastatic effect, CRC cells with angiotensin-activating ability were used in the mouse liver metastasis model. We suppressed AGT production in the mouse liver by using pro-AGT antisense S-ODN, which significantly suppressed the liver metastasis of CRC cells. Thus, CRC cells with angiotensin-activating ability are more likely to form liver metastasis. In CRC cases, A-II is associated with renin concentration in primary tumors[6]. Thus, high levels of A-II in primary CRC tissues, which indicates the potential to activate angiotensin in CRC cells, was associated with a high frequency of liver metastasis. The A-II concentra-

tion in primary CRC tissues may be a good marker for liver metastasis.

ANGIOTENSIN-TARGETING THERAPY FOR COLORECTAL CANCER

The renin/angiotensin-activating system is recognized as an important molecular target for CRC prevention and treatment. Several inhibitors of the renin/angiotensin-activating system suppress cancer development, cancer cell growth, angiogenesis, and metastasis[4,5,31-34]. Inhibitors of the renin-angiotensin system are widely used to treat hypertension. We have shown that some anti-angiotensin agents, inhibitors of renin and chymase, suppress liver metastasis of CRCs[6,35]. In addition, ACE inhibitors and/or A-II receptor blocker (ARB) have been reported to improve disease prognosis or progression in pancreatic and urogenital cancer[36,37].

We have also examined the combined effect of anti-angiotensin treatment and hypoglycemic treatment[35]. In a streptozotocin-induced BALB/c mouse diabetes model fed a high-calorie diet, the blood sugar level increased and was associated with increasing size and number of CT26 cell liver metastases. In this diabetes mouse model, we examined the effect of concurrent hypoglycemic and anti-angiotensin treatments[35]. Insulin and gliclazide (sulfonylurea) were administered with or without a renin inhibitor (aliskiren) to the liver metastasis mouse model fed a high-calorie diet and treated with streptozotocin injection. Treatment with insulin and gliclazide resulted in lower blood sugar levels compared to that in the untreated mice. The mice treated with insulin or gliclazide showed a decrease in the number of metastatic foci and improved survival compared to the untreated mice. Concurrent treatment with anti-angiotensin using aliskiren or captopril (ARB) and hypoglycemic agents (insulin or gliclazide) resulted in lower serum A-II concentration, fewer metastatic foci, and longer survival compared to the untreated mice or the mice treated with hypoglycemic agents alone. Combined treatment with anti-angiotensin and hypoglycemic agents showed a synergistic inhibitory effect on liver metastasis. The mice treated with the combination showed suppression of liver metastasis and improved survival, equal to that of the control mice.

Given that the association between hyperglycemia and liver metastasis in colon cancer is a result of renin upregulation, diabetes status is likely to be a risk factor for liver metastasis. Control of blood sugar could, therefore, be important in preventing liver metastasis in colon cancer patients. The use of anti-angiotensin treatment and blood sugar control as a baseline management for colon cancer patients with diabetes deserves to be examined in clinical trials in order to establish whether it helps in the prevention of liver metastasis (Figure 1).

CONCLUSION

As described above, the angiotensin activation is a pivotal feature of colorectal cancer for disease progression and liver metastasis. The angiotensin blockade and blood sugar control are hopeful tools for suppressing the liver metastasis of colorectal cancer. These treatments are provided commonly to patients of the hypertension and diabetes in an effective and safe manner. For CRC patients, especially, in their postoperative status, the angiotensin blockade and blood sugar control are relevant to prevent the liver metastasis in addition to the anti-cancer chemotherapy.

REFERENCES

1 Cancer Statistics in Japan, 2008. 2008 ed. Tokyo: National Cancer Center, 2008. Available from: URL: http: //ganjoho.jp/public/statistics/pub/statistics01.html
2 **Fujimoto Y**, Nakanishi Y, Sekine S, Yoshimura K, Akasu T, Moriya Y, Shimoda T. CD10 expression in colorectal carcinoma correlates with liver metastasis. *Dis Colon Rectum* 2005; **48**: 1883-1889
3 **Fong Y**, Kemeny N, Paty P, Blumgart LH, Cohen AM. Treatment of colorectal cancer: hepatic metastasis. *Semin Surg Oncol* 1996; **12**: 219-252
4 **Escobar E**, Rodríguez-Reyna TS, Arrieta O, Sotelo J. Angiotensin II, cell proliferation and angiogenesis regulator: biologic and therapeutic implications in cancer. *Curr Vasc Pharmacol* 2004; **2**: 385-399
5 **Wu XZ**. New strategy of antiangiogenic therapy for hepatocellular carcinoma. *Neoplasma* 2008; **55**: 472-481
6 **Shimomoto T**, Ohmori H, Luo Y, Chihara Y, Denda A, Sasahira T, Tatsumoto N, Fujii K, Kuniyasu H. Diabetes-associated angiotensin activation enhances liver metastasis of colon cancer. *Clin Exp Metastasis* 2012; **29**: 915-925
7 **Belova LA**. Angiotensin II-generating enzymes. *Biochemistry (Mosc)* 2000; **65**: 1337-1345
8 **Kumar R**, Singh VP, Baker KM. The intracellular renin-angiotensin system: implications in cardiovascular remodeling. *Curr Opin Nephrol Hypertens* 2008; **17**: 168-173
9 **Nishimura H**, Hoffmann S, Baltatu O, Sugimura K, Ganten D, Urata H. Angiotensin I converting enzyme and chymase in cardiovascular tissues. *Kidney Int Suppl* 1996; **55**: S18-S23
10 **Ferreira AJ**, Bader M, Santos RA. Therapeutic targeting of the angiotensin-converting enzyme 2/Angiotensin-(1-7)/Mas cascade in the renin-angiotensin system: a patent review. *Expert Opin Ther Pat* 2012; **22**: 567-574
11 Luo Y, Chihara Y, Fujii K, Matsushima S, Ohmori H, Hashizume A, Kuniyasu H. Expression of MAS1 in breast cancer in submission
12 **Iwai M**, Horiuchi M. Devil and angel in the renin-angiotensin system: ACE-angiotensin II-AT1 receptor axis vs. ACE2-angiotensin-(1-7)-Mas receptor axis. *Hypertens Res* 2009; **32**: 533-536
13 **Patey G**, De La Baume S, Schwartz JC, Gros C, Roques B, Fournie-Zaluski MC, Soroca-Lucas E. Selective protection of methionine enkephalin released from brain slices by enkephalinase inhibition. *Science* 1981; **212**: 1153-1155
14 **Shipp MA**, Vijayaraghavan J, Schmidt EV, Masteller EL, D'Adamio L, Hersh LB, Reinherz EL. Common acute lymphoblastic leukemia antigen (CALLA) is active neutral endopeptidase 24.11 ("enkephalinase"): direct evidence by cDNA transfection analysis. *Proc Natl Acad Sci USA* 1989; **86**: 297-301
15 **Yao T**, Takata M, Tustsumi S, Nishiyama K, Taguchi K, Nagai E, Tsuneyoshi M. Phenotypic expression of gastrointestinal differentiation markers in colorectal adenocarcinomas with liver metastasis. *Pathology* 2002; **34**: 556-560
16 **Ohji Y**, Yao T, Eguchi T, Yamada T, Hirahashi M, Iida M, Tsuneyoshi M. Evaluation of risk of liver metastasis in

colorectal adenocarcinoma based on the combination of risk factors including CD10 expression: multivariate analysis of clinicopathological and immunohistochemical factors. *Oncol Rep* 2007; **17**: 525-530
17 **Sumitomo M**, Shen R, Nanus DM. Involvement of neutral endopeptidase in neoplastic progression. *Biochim Biophys Acta* 2005; **1751**: 52-59
18 **Ogasawara M**, Murata J, Ayukawa K, Saimi I. Differential effect of intestinal neuropeptides on invasion and migration of colon carcinoma cells in vitro. *Cancer Lett* 1997; **116**: 111-116
19 **Boyella VD**, Nicastri AD, Bergasa NV. Human hepatic met-enkephalin and delta opioid receptor-1 immunoreactivities in viral and autoimmune hepatitis. *Ann Hepatol* 2008; **7**: 221-226
20 **Spivey JR**, Jorgensen RA, Gores GJ, Lindor KD. Methionine-enkephalin concentrations correlate with stage of disease but not pruritus in patients with primary biliary cirrhosis. *Am J Gastroenterol* 1994; **89**: 2028-2032
21 **Nicoll J**, Axiotis CA, Bergasa NV. The delta opioid receptor 1 is expressed by proliferating bile ductules in rats with cholestasis: implications for the study of liver regeneration and malignant transformation of biliary epithelium. *Med Hypotheses* 2005; **65**: 1099-1105
22 **Kuniyasu H**, Luo Y, Fujii K, Sasahira T, Moriwaka Y, Tatsumoto N, Sasaki T, Yamashita Y, Ohmori H. CD10 enhances metastasis of colorectal cancer by abrogating the anti-tumoural effect of methionine-enkephalin in the liver. *Gut* 2010; **59**: 348-356
23 **Skidgel RA**, Erdös EG. Angiotensin converting enzyme (ACE) and neprilysin hydrolyze neuropeptides: a brief history, the beginning and follow-ups to early studies. *Peptides* 2004; **25**: 521-525
24 **Nicolucci A**. Epidemiological aspects of neoplasms in diabetes. *Acta Diabetol* 2010; **47**: 87-95
25 **Larsson SC**, Orsini N, Wolk A. Diabetes mellitus and risk of colorectal cancer: a meta-analysis. *J Natl Cancer Inst* 2005; **97**: 1679-1687
26 **Saydah SH**, Platz EA, Rifai N, Pollak MN, Brancati FL, Helzlsouer KJ. Association of markers of insulin and glucose control with subsequent colorectal cancer risk. *Cancer Epidemiol Biomarkers Prev* 2003; **12**: 412-418
27 **Pais R**, Silaghi H, Silaghi AC, Rusu ML, Dumitrascu DL. Metabolic syndrome and risk of subsequent colorectal cancer. *World J Gastroenterol* 2009; **15**: 5141-5148
28 **Giovannucci E**. Metabolic syndrome, hyperinsulinemia, and colon cancer: a review. *Am J Clin Nutr* 2007; **86**: s836-s842
29 **Singh VP**, Baker KM, Kumar R. Activation of the intracellular renin-angiotensin system in cardiac fibroblasts by high glucose: role in extracellular matrix production. *Am J Physiol Heart Circ Physiol* 2008; **294**: H1675-H1684
30 **Dzau VJ**. Implications of local angiotensin production in cardiovascular physiology and pharmacology. *Am J Cardiol* 1987; **59**: 59A-65A
31 **Grossman E**, Messerli FH, Goldbourt U. Carcinogenicity of antihypertensive therapy. *Curr Hypertens Rep* 2002; **4**: 195-201
32 **Attoub S**, Gaben AM, Al-Salam S, Al Sultan MA, John A, Nicholls MG, Mester J, Petroianu G. Captopril as a potential inhibitor of lung tumor growth and metastasis. *Ann N Y Acad Sci* 2008; **1138**: 65-72
33 **Deshayes F**, Nahmias C. Angiotensin receptors: a new role in cancer? *Trends Endocrinol Metab* 2005; **16**: 293-299
34 **Fyhrquist F**, Saijonmaa O. Renin-angiotensin system revisited. *J Intern Med* 2008; **264**: 224-236
35 **Luo Y**, Ohmori H, Shimomoto T, Fujii K, Sasahira T, Chihara Y, Kuniyasu H. Anti-angiotensin and hypoglycemic treatments suppress liver metastasis of colon cancer cells. *Pathobiology* 2011; **78**: 285-290
36 **Nakai Y**, Isayama H, Ijichi H, Sasaki T, Sasahira N, Hirano K, Kogure H, Kawakubo K, Yagioka H, Yashima Y, Mizuno S, Yamamoto K, Arizumi T, Togawa O, Matsubara S, Tsujino T, Tateishi K, Tada M, Omata M, Koike K. Inhibition of renin-angiotensin system affects prognosis of advanced pancreatic cancer receiving gemcitabine. *Br J Cancer* 2010; **103**: 1644-1648
37 **Miyajima A**, Kikuchi E, Kosaka T, Oya M. Angiotensin II Type 1 Receptor Antagonist as an Angiogenic Inhibitor in Urogenital Cancer. *Rev Recent Clin Trials* 2009; **4**: 75-78

S- Editor Jiang L **L- Editor** Kerr C **E- Editor** Lu YJ

Comparison of effects of a selective 5-HT reuptake inhibitor versus a 5-HT $_4$ receptor agonist on in vivo neurogenesis at the rectal anastomosis in rats

Isao Kawahara, Hiroki Kuniyasu, Hiroko Matsuyoshi, Kei Goto, Koji Obata, Hiromi Misawa, Hisao Fujii and Miyako Takaki

Am J Physiol Gastrointest Liver Physiol 302:G588-G597, 2012. First published 22 December 2011; doi:10.1152/ajpgi.00284.2011

AJP - Gastrointestinal and Liver Physiology publishes original articles pertaining to all aspects of research involving normal or abnormal function of the gastrointestinal tract, hepatobiliary system, and pancreas. It is published 12 times a year (monthly) by the American Physiological Society, 9650 Rockville Pike, Bethesda MD 20814-3991. ISSN: 0193-1857, ESSN: 1522-1547. Visit our website at http://www.the-aps.org/.

Am J Physiol Gastrointest Liver Physiol 302: G588–G597, 2012.
First published December 22, 2011; doi:10.1152/ajpgi.00284.2011.

Comparison of effects of a selective 5-HT reuptake inhibitor versus a 5-HT_4 receptor agonist on in vivo neurogenesis at the rectal anastomosis in rats

Isao Kawahara,[1] Hiroki Kuniyasu,[2] Hiroko Matsuyoshi,[1] Kei Goto,[1] Koji Obata,[1] Hiromi Misawa,[1] Hisao Fujii,[3] and Miyako Takaki[1]

Departments of [1]Physiology II, [2]Molecular Pathology, and [3]Surgery, Nara Medical University School of Medicine, Kashihara, Japan

Submitted 21 July 2011; accepted in final form 19 December 2011

Kawahara I, Kuniyasu H, Matsuyoshi H, Goto K, Obata K, Misawa H, Fujii H, Takaki M. Comparison of effects of a selective 5-HT reuptake inhibitor versus a 5-HT_4 receptor agonist on in vivo neurogenesis at the rectal anastomosis in rats. *Am J Physiol Gastrointest Liver Physiol* 302: G588–G597, 2012. First published December 22, 2011; doi:10.1152/ajpgi.00284.2011.—It was recently reported that activation of enteric neural 5-HT_4 receptors (SR4) promotes reconstruction of enteric neural circuit injury in distal gut of guinea pigs and that this reconstruction involves neural stem cells. We aimed to explore a novel approach using a selective serotonin reuptake inhibitor (SSRI), which increases endogenous 5-HT, to repair enteric nerve fiber injury in the rat distal gut. Enteric nerve fiber injury was performed by rectal transection and subsequent end-to-end one-layer anastomosis. The SSRI fluvoxamine maleate (100 μmol/l) was applied locally at the anastomotic site to compare with the 5-HT_4 agonist mosapride citrate (100 μmol/l) (applied for patent) applied locally and orally. Unlike mosapride, fluvoxamine failed to promote the regeneration of the nerve fiber tract across the anastomosis. Furthermore, fluvoxamine did not generate anti-distal-less homeobox 2 (DLX2)- and anti-SR4-positive cells (neural stem cells) and/or anti-neurofilament (NF)-positive cells (neural cells) in newly formed granulation tissue at the anastomosis, whereas these cell types were observed in mosapride-treated preparations. In contrast to its effects in guinea pigs, mosapride generated 5-bromo-2′-deoxyuridine (BrdU)-positive neural cells in ganglia sites 3 mm oral and anal from the anastomosis 2 wk after nerve fiber injury. All actions of mosapride were observed after local and or oral applications. These findings indicate that local SSRI treatment does not induce in vivo nerve fiber tract growth across the anastomosis in the rat distal gut. Mosapride induces nerve fiber tract growth across the anastomosis, mediated through enteric neural stem cells possibly from neural crest-derived stem cells or mesenchymal stem cells in the bone marrow.

selective serotonin reuptake inhibitor; neural stem cell; serotonin-4 receptor; enteric nervous system

THE ENTERIC NERVOUS SYSTEM (ENS), which is composed of the neurons and nerve fibers in the gastrointestinal tract, has independent intrinsic reflex circuits regulating motility and secretion, although it exhibits many features resembling the central nervous system (CNS) (5). Enteric neurons are as phenotypically diverse as those of the CNS and include a variety of neurotransmitters found in the CNS, and the number of neurons in the ENS is equivalent to that in the spinal cord (5). Recently, we reported that brain-derived neurotrophic factor (BDNF) induces the formation of enteric neural networks from murine embryonic stem (ES) cells (21). Furthermore, we found that after rectal transection local in vivo application of BDNF improved distension-evoked reflexes of the internal anal sphincter (IAS) (6). We also demonstrated that BDNF facilitates the regeneration of the reflex nerve pathway and enteric neurogenesis from neural stem cells in the granulation tissue at the anastomotic site (6). As a repairing mechanism for the neural circuit insult, we suggested that the neural stem cells have a pivotal role in enteric neurogenesis.

We have also found that a 5-HT_4 receptor agonist, mosapride (MOS), enhances in vivo the defecation reflex composed of the intrinsic rectal cholinergic contraction reflex and IAS nitrergic relaxation reflexes mediated through physiologically active enteric neural 5-HT_4 receptors in guinea pigs (9, 10, 19). It has also been reported that 5-HT_4 receptor stimulation increases neuronal numbers and the length of neurites in enteric neurons developing in vitro from immunoselected neural crest-derived precursors (12). As further support for a role of 5-HT_4 receptors we have demonstrated that enteric neural 5-HT_4 receptor stimulation promotes in vivo reconstruction of an enteric neural circuit, leading to the recovery of the impaired defecation reflex in the distal gut in guinea pigs, and that this reconstruction possibly involves neural stem cells (15, 16, 28). Consistent with this finding, 5-HT_4 receptor-mediated neuroprotection and neurogenesis in the ENS have been shown in adult mice (13).

5-HT can stimulate 5-HT_4 receptors (20) as well as other subtypes of 5-HT receptors. Selective serotonin reuptake inhibitors (SSRIs) are widely used as antidepressants. SSRIs can increase endogenous 5-HT in the gastrointestinal tract (1). The endogenous 5-HT increased by SSRI can act on enteric neural 5-HT_4 receptors, as well as other subtypes of 5-HT receptors (14). We therefore compared the abilities of the 5-HT_4 receptor agonist MOS and the SSRI fluvoxamine maleate to promote neurogenesis from nerve fiber tract injury in rats. We also evaluated effects of local application (MOS-LA) versus oral

Address for reprint requests and other correspondence: M. Takaki, Dept. of Physiology II, Nara Medical Univ., 840 Shijo-cho, Kashihara 634-8521, Japan (e-mail: mtakaki@naramed-u.ac.jp).

application (MOS-PO) of MOS in rats to explore the possibility of clinical application.

METHODS

Animal preparation. All surgical and experimental procedures were performed according to the *Guide for the Care and Use of Laboratory Animals* published by the National Institutes of Health (NIH Pub. No. 85-23, revised 1996) and were reviewed and approved by the animal care and use committee of Nara Medical University. The abdomens of 45 male rats (body wt: 300–500 g) were opened by lower midline laparotomy under anesthesia with Nembutal (40 mg/kg ip). This surgical approach was performed to spare extrinsic inputs from the lumbar colonic nerves. Rectal transection (RT) 4 cm from the anal verge and an end-to-end one-layer rectal anastomosis (RA) were performed. Local treatment with vehicle [0.1% dimethyl sulfoxide (DMSO), Control; n = 5 rats], fluvoxamine (SSRI, 100 μmol/l; n = 9 rats), or MOS (100 μmol/l; n = 6 rats) at the anastomotic site was performed by application of gelatin sponge (GS) [W × L: 0.6 cm × 1.6 cm; each upper half (0.8 cm) and lower half (0.8 cm) was wrapped around the anastomotic site; soaked solution volume = 0.1 ml] (n = total of 20 rats) right after surgery. GS was inserted tightly between the rectum and the seminal vesicle. This GS was not completely absorbed until 4 wk after application.

Additional experiments involved subcutaneous implantation of GS (W × L: 0.5 cm × 0.5 cm; thickness: 0.25 cm) at the neck for 3 days. GS was treated with 0.1 ml of 0.1% DMSO (n = 5 rats), 100 μmol/l MOS (n = 5 rats), 100 μmol/l SSRI (n = 5 rats), or 50 μmol/l GR113808 (GR) + 100 μmol/l MOS (n = 3 rats). GS was removed for immunohistochemistry and quantitative reverse transcription-polymerase chain reaction (qRT-PCR).

In some experiments, MOS [MOS-PO: concentration and volume of MOS were 100 μmol/l and 50 ml/day (n = 15 rats), corresponding to 1 $mg \cdot kg^{-1} \cdot day^{-1}$] or 0.1% DMSO solution (Cont-PO; n = 10 rats) was added to the drinking water. We checked the decrease in the weight of the bottle containing MOS solution daily.

Measurement of defecation reflex. Experiments were performed on nine male guinea pigs (5 for MOS and 4 for SSRI; body wt: 330–430 g) anesthetized with ethyl carbamate (0.7–1.0 g/kg ip), artificially ventilated, and immobilized with gallamine (0.1 mg/kg iv). Two weeks after RT and RA, rectal motility was recorded with a warm water-filled balloon that was attached to flexible polyethylene tubing connected to a pressure transducer. The 1.5-cm-long balloon was introduced into the rectum 5 cm oral to the anus. Gradual and sustained rectal distension for 5 min at intervals of 20 min was performed as previously reported (6, 9, 15, 29).

The motility of the IAS was recorded with a custom-made strain gauge force transducer similar to that described previously (6, 9, 15, 29). The reflex response composed of recto-rectal (R-R) and recto-internal anal sphincter (R-IAS) reflexes was evaluated by "reflex index" as previously reported (15).

Drugs. The following drugs were used: fluvoxamine maleate (SSRI; Wako Pure Chemical Industries, Osaka, Japan), mosapride citrate (MOS; kindly donated by Dainippon-Sumitomo Pharmaceutical, Osaka, Japan), GR113808 (GR; Wako Pure Chemical Industries), gallamine triethiodide (Sigma, St. Louis, MO), and ethyl carbamate (Wako Pure Chemical Industries). MOS, SSRI, and GR dissolved in a solution containing 100% DMSO were diluted to 1,000-fold with a final DMSO concentration of 0.1%. This concentration of DMSO did not exert any effects on experimental results.

Immunohistochemistry. The rectal whole mount preparations were fixed in 4% paraformaldehyde (4°C, overnight) or 99.5% acetone (4°C, 1 h) to detect neurofilament (NF) or neuronal nitric oxide synthase (nNOS). Thereafter, the mucosa and submucosa were removed from respective preparations, which were washed for 30 min in PBS (0.01–0.1 mol/l, pH 7.4) and then incubated for 3–12 h at 4°C in 10% normal donkey serum in PBS containing 0.3% (vol/vol) Triton X-100 (PBS-TX) to reduce nonspecific antibody binding. After incubation for 2 days at 4°C with a rabbit polyclonal antiserum cocktail to label NF (clone 2F11, reacting with 70-, 160-, and 200-kDa proteins, 0.5 μg/ml; DAKO) (21) or with a goat polyclonal antibody to label NOS (ProSci, Poway, CA) (5), NF and nNOS immunoreactivities were detected with Alexa Fluor 594- and Alexa Fluor 488-conjugated secondary antibody, respectively. Tissues were examined with an Olympus FV1000 (Tokyo, Japan) confocal microscope. Confocal micrographs are digital composites of Z-series scans of 10–15 optical sections through a depth of 10–20 μm or 100–150 μm. Final images were constructed with the FV10-ASW software application (version 1.7, Olympus).

For immunohistochemistry of sectioned preparations, the rectum including an anastomotic site and GS was fixed with 4% paraformaldehyde at 4°C and embedded in paraffin. Consecutive 4-μm sections were cut from each block. Immunostaining was performed by the immunoperoxidase technique after antigen retrieval with microwave treatment (15 min twice in pH 6.0 citrate buffer) for proliferating cell nuclear antigen (PCNA) and treatment with pepsin (DAKO, Carpinteria, CA) for 20 min at room temperature for distal-less homeobox 2 (DLX2), serotonin receptor 4 (SR4), and NF or c-RET. After endogenous peroxidase blockade with 3% H_2O_2-methanol for 15 min, specimens were rinsed with PBS and incubated with a primary antibody diluted with washing solution (BioGenex, San Ramon, CA) at room temperature for 2 h, as previously reported (6, 16). The specimens were rinsed with PBS and incubated at room temperature for 1 h with secondary antibody conjugated to peroxidase diluted at 0.5 μg/ml (Medical & Biotechnological Laboratories, Nagoya, Japan). The sections were then rinsed with PBS, color-developed with diaminobenzidine (DAB) solution (DAKO), and counterstained with Mayer's hematoxylin (Sigma). Antibodies used in primary reaction and working concentrations were as follows: anti-NF (clone 2F11, reacting with 70-, 160-, and 200-kDa proteins, 0.5 μg/ml; DAKO) (21), anti-SR4 (clone N-16; the epitope is located at the N-terminus of human SR4, 0.5 μg/ml; Santa Cruz Biotechnology, Santa Cruz, CA) (16), and anti-DLX2 (catalog no. ab18188, 0.5 μg/ml; Abcam, Tokyo, Japan) (6, 16, 27) as enteric neural stem cell markers, anti-PCNA (clone PC10; DAKO) as a cell proliferating marker that is specifically expressed in cell nuclei during the S phase (3), and anti-c-RET (rabbit polyclonal, 2 μg/ml; Assay Biotechnology, Sunnyvale, CA) as a neural crest-derived stem cell marker.

Quantitative reverse transcription-polymerase chain reaction. Extraction of total RNA was carried out with the RNeasy Mini Kit (Qiagen Genomics, Bothell, WA), and total RNA (1 μg) was synthesized with the ReverTra Ace-a-RT Kit (Toyobo, Osaka, Japan). qRT-PCR was performed by StepOne Real-Time PCR Systems (Applied Biosystems, Foster City, CA) using Fast SYBR Green Master Mix (Applied Biosystems) and analyzed by the relative standard curve quantification method. PCR condition was set according to the provider's instructions. ACTB mRNA was amplified for internal control (GenBank accession no. NM001101). Each amplification reaction was evaluated by a melting curve analysis. For visualizing PCR products, agarose gel electrophoresis was performed with ethidium bromide staining.

Primer sets were upper 5′-ACT CAT GCC CAT TTC CT-3′ and lower 5′-AGG AAA TGG GCA TGA GT-3′ for mouse SR4 (NM_012853.1), upper 5′-TCC TAC TCC GCC AAA AG-3′ and lower 5′-GCC CGC CAT CCG CTG TT-3′ for mouse DXL2 (NM_001191746.1), upper 5′-CGG ACG CGT GGG CAG CC-3′and lower 5′-GGC TGC CCA CGC GTC CG-3′ for mouse NF (NM_017029.1), upper 5′-CCA AAT CAA GAG AAA GT-3′ and lower 5′-TCA GAG CAA AAG TTA GC-3′ for mouse PCNA (NM_022381.3), and upper 5′-GCG CCC CGA GTG TGA GG-3′ and lower 5′-CCT CAC ACT CGG GGC GC-3′ for mouse c-Ret (AF042830.2).

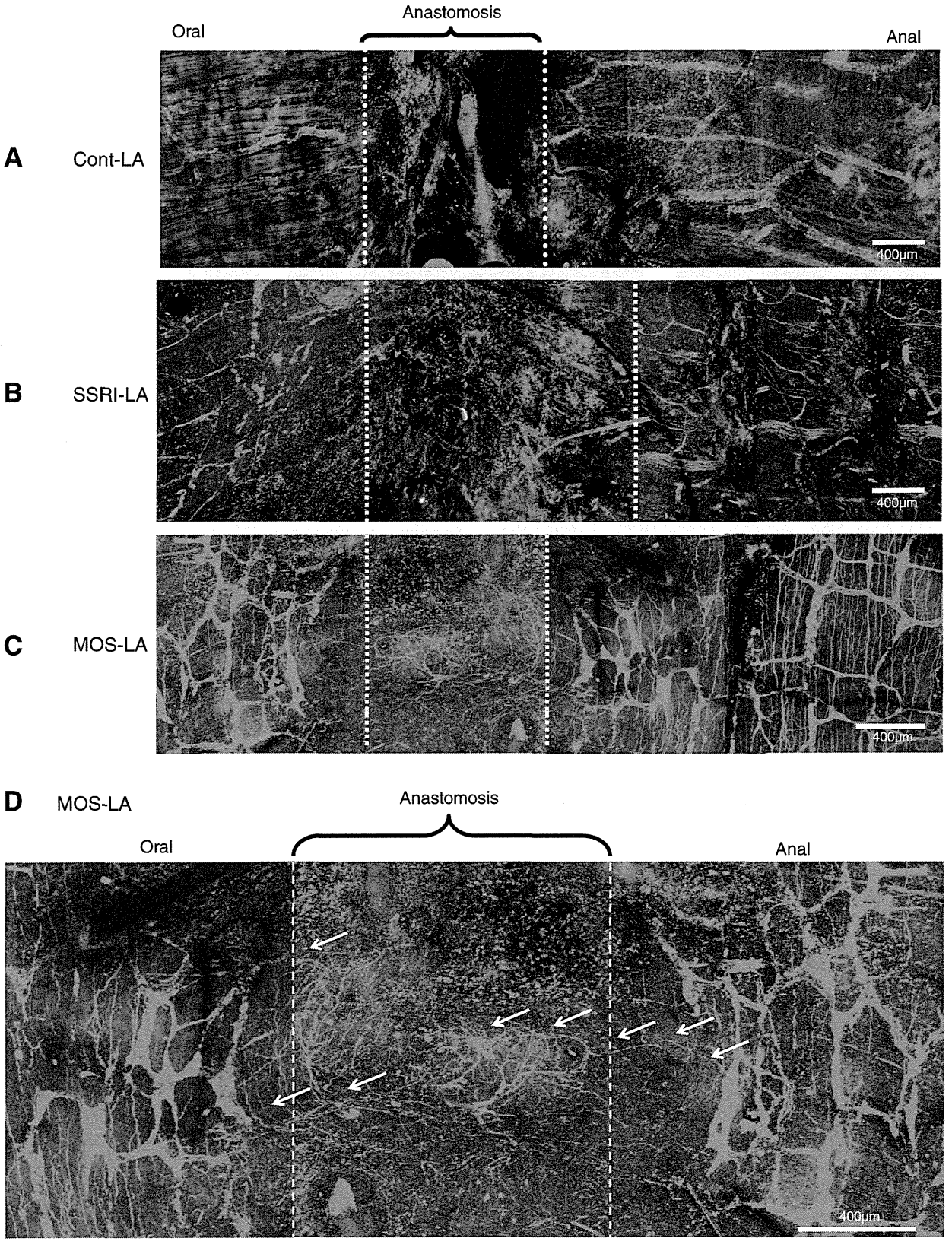

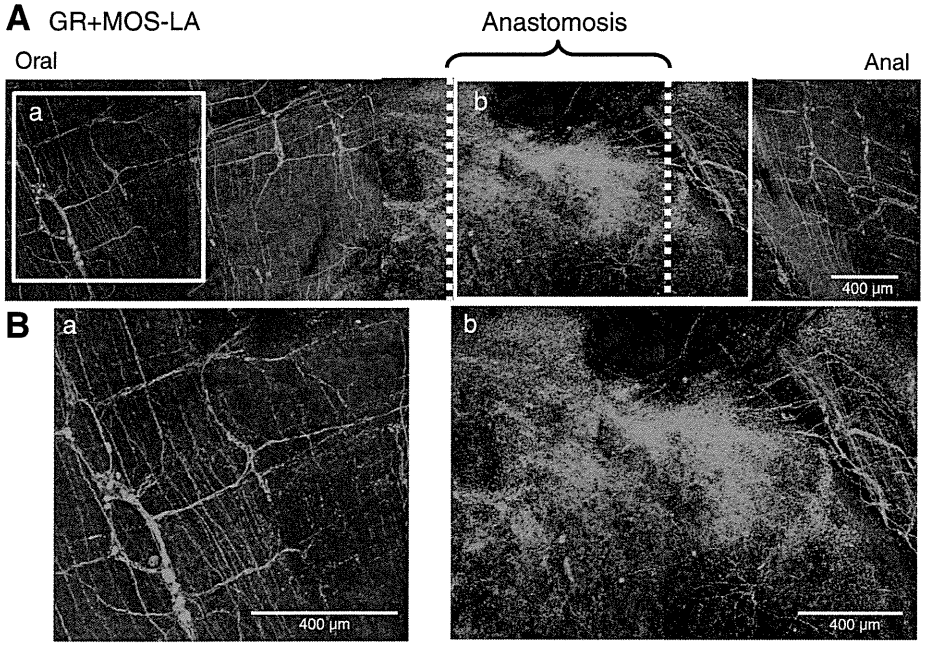

Fig. 2. Immunostaining for NF in the rectal myenteric plexus 2 wk after RT+RA treated with 50 μmol/l GR113808 (GR) + 100 μmol/l MOS-LA. *A*: nerve fibers are not present in the anastomotic region (*b*), although the intact myenteric plexus can be seen (*a*). *B*, *a* and *b*: enlarged views of areas enclosed in yellow boxes in *Aa* and *Ab*, respectively.

Detection of regenerated enteric neurons. To identify neuronal cell proliferation, 5-bromo-2-deoxyuridine (BrdU, 1 mg/ml solution; Sigma or Nacalai Tesque, Kyoto, Japan) was added to the drinking water for 1–2 wk for 12 animals: 2 were fluvoxamine treated by LA, 2 and 3 were MOS treated by LA and PO, and 2 and 3 were 0.1% DMSO treated by LA and PO. After rinsing in PBS, the specimens were pretreated with sodium chloride-sodium citrate solution for 2 h at 65°C, followed by partial denaturation of double-stranded DNA with 2 mol/l HCl for 30 min at 37°C. To reveal BrdU, the sections were incubated with a rat monoclonal antibody raised against BrdU (Abcam) overnight at 4°C. The specimens were rinsed in 0.1 mol/l Tris-EDTA (pH 7.8), followed by routine immunohistochemistry.

Statistical analysis. Statistical significance of differences between means was determined by Mann-Whitney *U*-test or one way- or two-way ANOVA, followed by multiple comparisons by Bonferroni or Fisher's protected least significant difference (PLSD) post hoc test. A P value of <0.05 was considered statistically significant.

RESULTS

Effects of fluvoxamine and mosapride by local application on regeneration of NF- and nNOS-positive fibers after nerve fiber tract injury. Myenteric neurons in the rectal anastomotic site were severely damaged and the neural network was disrupted after 2 wk, although myenteric neurons at oral and anal sites of the anastomotic site appeared to be intact after treatment with vehicle and the SSRI fluvoxamine (Fig. 1, *A* and *B*). However, after treatment with MOS for 2 wk, bundles of fine nerve fibers were observed traversing the oral and anal ends of the myenteric plexus, as previously described in guinea pigs (15, 16) (Fig. 1, *C* and *D*).

In contrast, in the rectal anastomotic site treated with GR and MOS for 2 wk, these patterns of new axon growth were not observed (Fig. 2, *Ab* and *Bb*).

Additional effects of SSRI and MOS-LA on anti-PCNA-, DLX2-, SR4-, and NF-positive cells in granulation tissue sections at anastomotic site 1–2 wk after nerve fiber tract injury. The granulation tissue defined as new tissue formed by growth of fibroblasts and blood capillaries into injured tissue was newly formed at the rectal anastomotic site 1–2 wk after RT + RA. In the granulation tissue at the anastomotic site treated with SSRI or MOS for 1–2 wk, myenteric networks observed in the intact rectal region were absent in the region within 1–3 mm of the anastomosis, consistent with observations in the whole mount preparations.

In the granulation tissue at the rectal anastomotic site treated with SSRI, after 1–2 wk PCNA-positive cells were observed as in the tissue treated with MOS but DLX2-, SR4-, and NF-positive cells were only observed sparsely in the tissue treated with SSRI (Fig. 3, *A* and *B*).

After 1–2 wk, PCNA-positive cells including fibroblasts with proliferating activity were frequently found in the granulation tissue within the anastomotic site treated with SSRI (83 ± 18 and 72 ± 16 cells/mm^2) and MOS (72 ± 11 and 47 ± 6 cells/mm^2) (Fig. 3*C*). However, after 1 wk, cells immunoreactive for DLX2 and SR4 were significantly diminished in the granulation tissue treated with SSRI compared with MOS [16 ± 4 vs. 42 ± 5 cells/mm^2 ($P < 0.05$) and 6 ± 2 vs. $12 \pm$

Fig. 1. Immunostaining for neurofilament (NF) in the rectal myenteric plexus 2 wk after rectal transection and rectal anastomosis (RT+RA). Nerve fibers are not present in the anastomotic region 2 wk after local treatment with vehicle (Cont-LA; *A*). After treatment with fluvoxamine (SSRI-LA; 100 μmol/l), nerve fibers are absent from the anastomotic site (*B*). SSRI caused inflammatory responses, resulting in hypertrophied anastomosis. After local treatment with mosapride (MOS-LA; 100 μmol/l), fine nerve fibers can be seen across the anastomosis between the oral and anal cut ends of the myenteric plexus as shown by arrows (*C*; anastomotic region is enlarged in *D*).

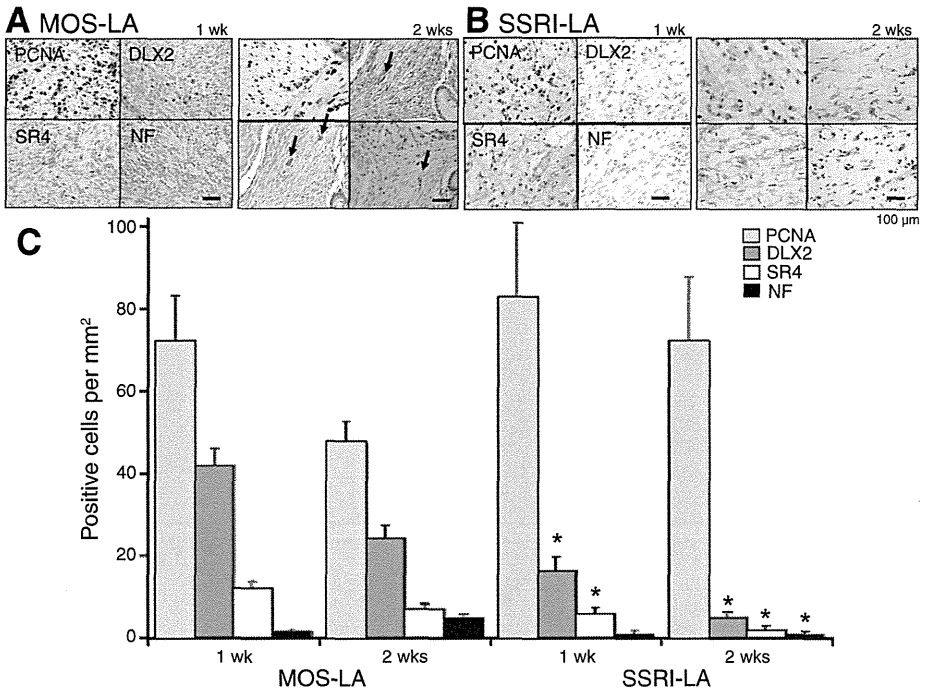

Fig. 3. Representative set of images of immunostaining for proliferating cell nuclear antigen (PCNA), distal-less homeobox 2 (DLX2), serotonin receptor 4 (SR4), and NF. Representative images of immunostaining for PCNA, DLX2, NF, and SR4 at the anastomotic site treated with MOS-LA (*A*) and SSRI-LA (*B*) for 1 wk and 2 wk after RT+RA are shown. PCNA-positive cells were detected similarly in *A* and *B*, but DLX2-, SR4-, and NF- positive cells were less detected in the granulation tissue within the anastomotic site after SSRI-LA (*B*). In particular, SR4- and NF-positive cells were not detected 2 wk after SSRI-LA (*B*, *right*) but were detected as indicated by arrows after MOS-LA (*A*, *right*). Calibration bars, 100 μm. *C*: summarized effects of MOS-LA and SSRI-LA on numbers of PCNA-, DLX2-, SR4-, and NF-positive cells in the granulation tissue within 2 mm of anastomotic site. Mean values were obtained from 5 high-powered fields (HPFs; 0.2 mm^2). *$P < 0.05$ vs. MOS-LA by Mann-Whitney *U*-test.

2 cells/mm^2 ($P < 0.05$)]. After 2 wk cells immunoreactive for DLX2, SR4, and NF were less dense in the granulation tissue treated with SSRI compared with MOS [5 ± 2 vs. 24 ± 3 cells/mm^2 ($P < 0.05$), 2 ± 1 vs. 7 ± 1 cells/mm^2 ($P < 0.05$), and 1 ± 1 vs. 5 ± 1 cells/mm^2; ($P < 0.05$)] (Fig. 3*C*). Therefore, in the granulation tissue treated with SSRI, no neural stem cells and no neurons were found, different from the tissue treated with MOS.

Comparison of effects of MOS and SSRI on mobilization of anti-PCNA-, DLX2-, SR4-, and c-RET-positive cells into subcutaneously implanted GS at the neck. MOS significantly increased the number of DLX2-, SR4-, and c-RET-positive cells in the implanted GS, but SSRI markedly decreased the number of DLX2- and SR4-positive cells compared with control and MOS (Fig. 4), like SSRI applied at the anastomotic site (Fig. 3). No NF-positive cells were observed. DLX2- and SR4-positive cells are neural stem cells, and c-RET-positive cells are neural crest-derived stem cells (21). Therefore, it seems likely that MOS differentiates neural crest-derived stem cells (17) or mesenchymal stem cells mobilized from the bone marrow into neural stem cells and that SSRI suppresses mobilization of neural crest-derived stem cells or mesenchymal stem cells and/or differentiation into neural stem cells. These results were confirmed by similar results by qRT-PCR (Fig. 5). In addition, GR antagonized MOS-induced increases of mRNA of DLX2, SR4, and c-RET to 0.92 ± 0.43-fold, 1.14 ± 0.34-fold, and 1.18 ± 0.21-fold of control, respectively.

Comparison of effects of LA vs. PO delivery of MOS on regeneration of NF- and nNOS-positive fibers after nerve fiber tract injury. After treatment with 0.1% DMSO by oral application for 2 wk, no bundles of fine nerve fibers were observed within the anastomotic site (Fig. 6*A*). However, after treatment with MOS-PO for 2 wk, fine nerve fibers were observed traversing the oral and anal ends of the myenteric plexus (Fig. 6*Ba*) as after MOS-LA for 2 wk (Fig. 1, *C* and *D*). nNOS-positive fine nerve fibers were also observed (Fig. 6*Bb*).

BrdU-positive cells were identified in sites 3 mm oral and anal from the anastomotic sites treated for 2 wk with MOS-LA (Fig. 7*A*) and MOS-PO (Fig. 7*B*), unlike in guinea pigs (16). Summarized data of BrdU positivity indicated that MOS-PO significantly increased BrdU-positive cells from MOS-LA in 5 mm oral and 5 mm anal sites but not in 3 mm oral and 3 mm anal sites (Fig. 7*C*). In contrast, SSRI-LA showed significantly less BrdU immunoreactivity in all sites (Fig. 7*C*). Although BrdU-positive cells also appeared to include fibroblasts, endothelial cells, and macrophages, BrdU-positive cells forming ganglia include newly formed neurons.

Comparison of additional effects of MOS on anti-PCNA-, DLX2-, SR4-, and NF-positive cells in granulation tissue sections at anastomotic site 1–2 wk after nerve fiber tract injury between PO and LA. After 1–2 wk, PCNA-positive cells were frequently found in the granulation tissue within the anastomotic site in preparations from animals treated with MOS-PO and MOS-LA, although PCNA-positive cells decreased after 2 wk. Cells immunoreactive for DLX2, SR4, and NF were also frequently found in the granulation tissue treated with MOS-PO and MOS-LA, but DLX2-, SR4-, and NF-positive cells after 1 wk were more frequently found in the tissue treated with MOS-PO than in that treated with MOS-LA. After 2 wk, the appearance of DLX2-, SR4-, and NF-positive cells was comparable in the tissues treated with MOS-PO and MOS-LA (Fig. 8, *A* and *B*). SR4-positive cells in the tissues treated with MOS-PO were found in a ganglion (Fig. 8*B*).

After 1–2 wk, the number of PCNA-positive cells was similar in granulation tissue within the anastomotic site in preparations from animals treated with MOS-PO (72 ± 10 and 38 ± 5) and MOS-LA (72 ± 11 and 47 ± 6). The number of cells immunoreactive for DLX2, SR4, and NF was signifi-

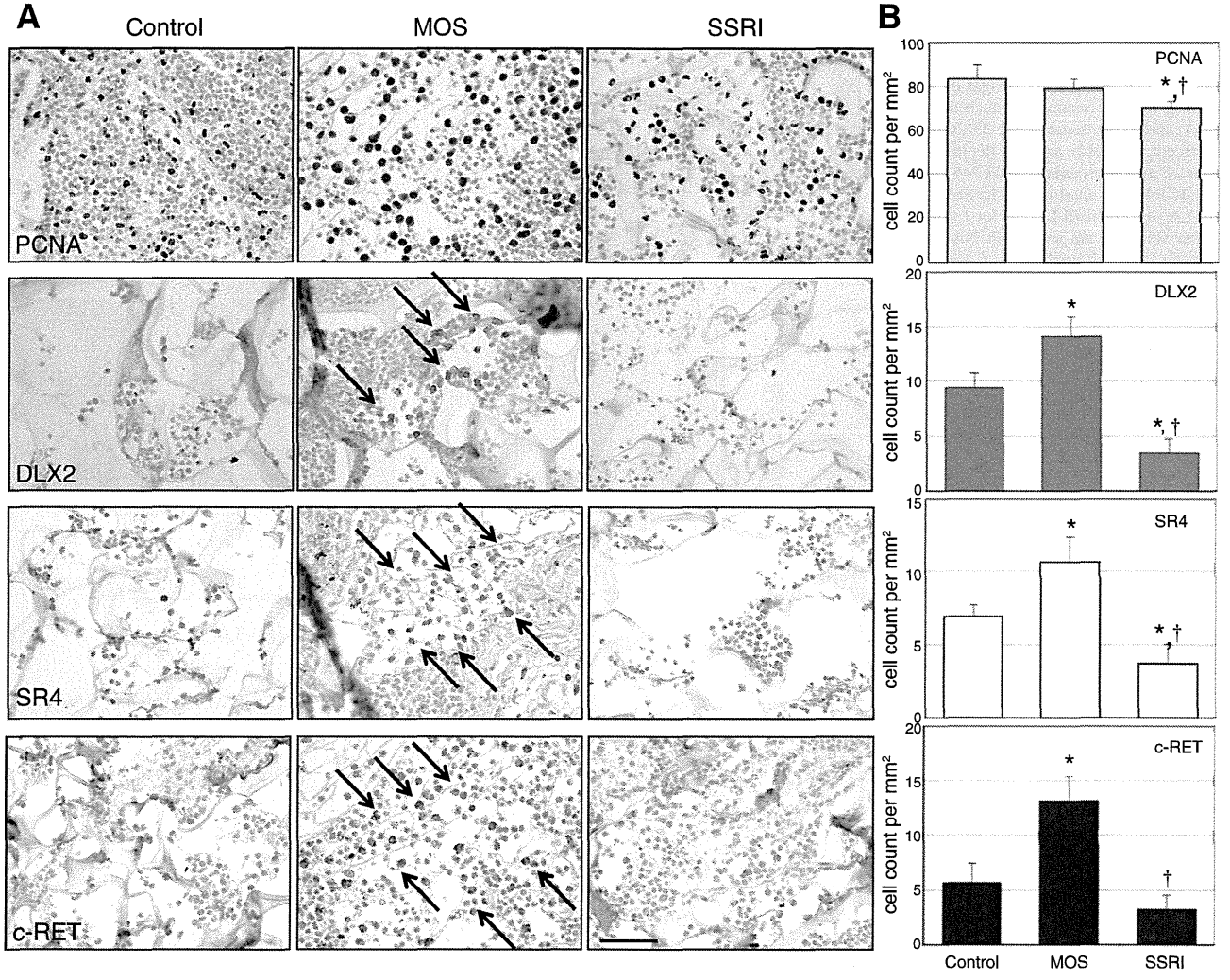

Fig. 4. Immunostaining for PCNA, DLX2, SR4, and c-RET after 3 days following the subcutaneous implantation of gel sponge at the neck. *A*: representative images of immunostaining for PCNA, DLX2, SR4, and c-RET after 3 days following the subcutaneous implantation of gel sponge (W × L: 0.5 cm × 0.5 cm; thickness: 0.25 cm) at the neck. Gel sponge absorbed 0.1% DMSO (Control), 100 μmol/l MOS, and 100 μmol/l SSRI. Calibration bar, 100 μm. *B*: summarized effects of Control, MOS, and SSRI on numbers of PCNA-, DLX2-, SR4-, and c-RET-positive cells in the gel sponge. Mean values were obtained from 10 HPFs (0.2 mm^2). *$P < 0.05$ vs. Control, †$P < 0.05$ vs. MOS by Mann-Whitney *U*-test.

cantly larger in granulation tissue treated with MOS-PO than in that treated with MOS-LA after 1 wk [54 ± 5 vs. 42 ± 5 ($P < 0.05$), 18 ± 2 vs. 12 ± 2 ($P < 0.05$), and 9 ± 2 vs. 2 ± 0 ($P < 0.05$)] (Fig. 8*C*). However, there were no significant differences in the number of DLX2-, SR4-, and NF-positive cells between MOS-PO and MOS-LA after 2 wk except for the number of SR4-positive cells (Fig. 8*C*).

Measurement of defecation reflex. Figure 9*A* shows representative examples of R-R and R-IAS reflex recoveries at 2 wk after nerve fiber tract injury in a guinea pig treated with MOS-LA. In contrast, the R-IAS reflex response remained abolished and the R-R reflex was unchanged in a guinea pig treated with SSRI-LA (Fig. 9*B*). Mean reflex index of R-IAS reflex was 0 for SSRI-LA ($n = 4$), whereas it was ~0.8 for MOS-LA ($n = 5$) (15).

DISCUSSION

The results reported here indicate that SSRI does not induce in vivo nerve fiber tract growth across a surgical anastomosis, but MOS-LA and MOS-PO promoted a 5-HT_4 receptor-mediated neural regeneration, since effects of MOS-LA and MOS-PO were antagonized by 5-HT_4 receptor antagonists GR (see Fig. 2) and SB-207266 (our unpublished data in guinea pigs and mice), respectively. There were no significant differences in nerve fiber tract growth action between MOS-LA and MOS-PO after 2 wk, suggesting that the clinical application of MOS is promising.

SSRI can increase endogenous 5-HT in the gastrointestinal tract (1). Increased endogenous 5-HT can act on enteric neural 5-HT_4 receptors as well as other subtypes of 5-HT receptors such as 5-HT_3 receptors (14). In fact, there is evidence supporting the idea that a variety of subtypes of 5-HT receptors play roles in the inflammatory response (2, 7, 26). 5-HT_3 receptors in in vitro nodose ganglion play proinflammatory roles (7), whereas enteric neuronal 5-HT_4 receptors induce anti-inflammatory actions via α7nACh receptors on muscularis macrophages associated with postop-

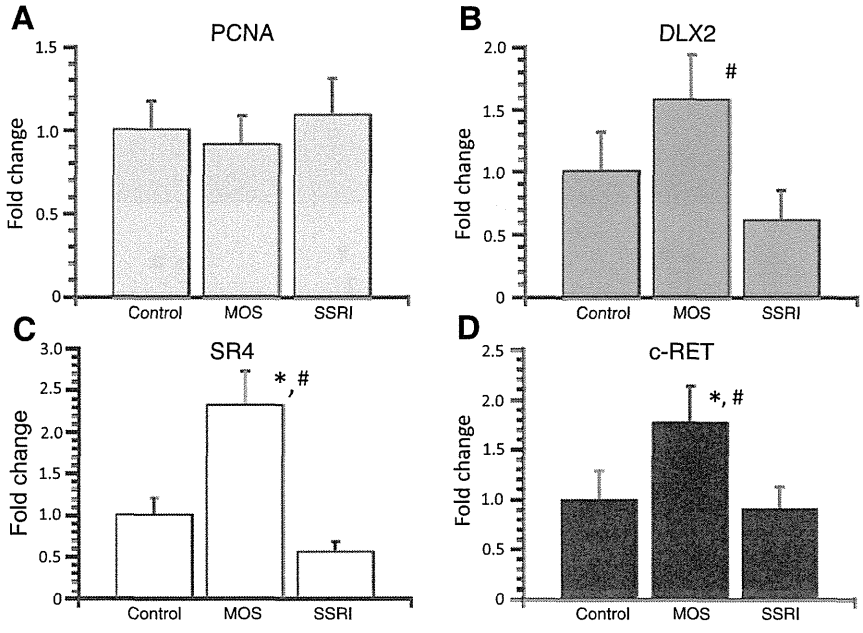

Fig. 5. qRT-PCR analysis for mRNA of PCNA, DLX2, SR4, and c-RET after 3 days following the subcutaneous implantation of gel sponge at the neck. Gel sponge absorbed 0.1% DMSO (Control), 100 μmol/l MOS, 100 μmol/l SSRI, and 50 μmol/l GR + 100 μmol/l MOS. *A*: PCNA mRNA. *B*: DLX2 mRNA. *C*: SR4 mRNA. *D*: c-RET mRNA. GR antagonized effects of MOS. NF mRNA was not detected. $*P < 0.05$ vs. Control by Fisher's protected least significant difference (PLSD) post hoc test in *D* and by Bonferroni post hoc test in *C*. $\#P < 0.05$ vs. SSRI by Fisher's PLSD post hoc test in *B* and *D* and by Bonferroni post hoc test in *C*.

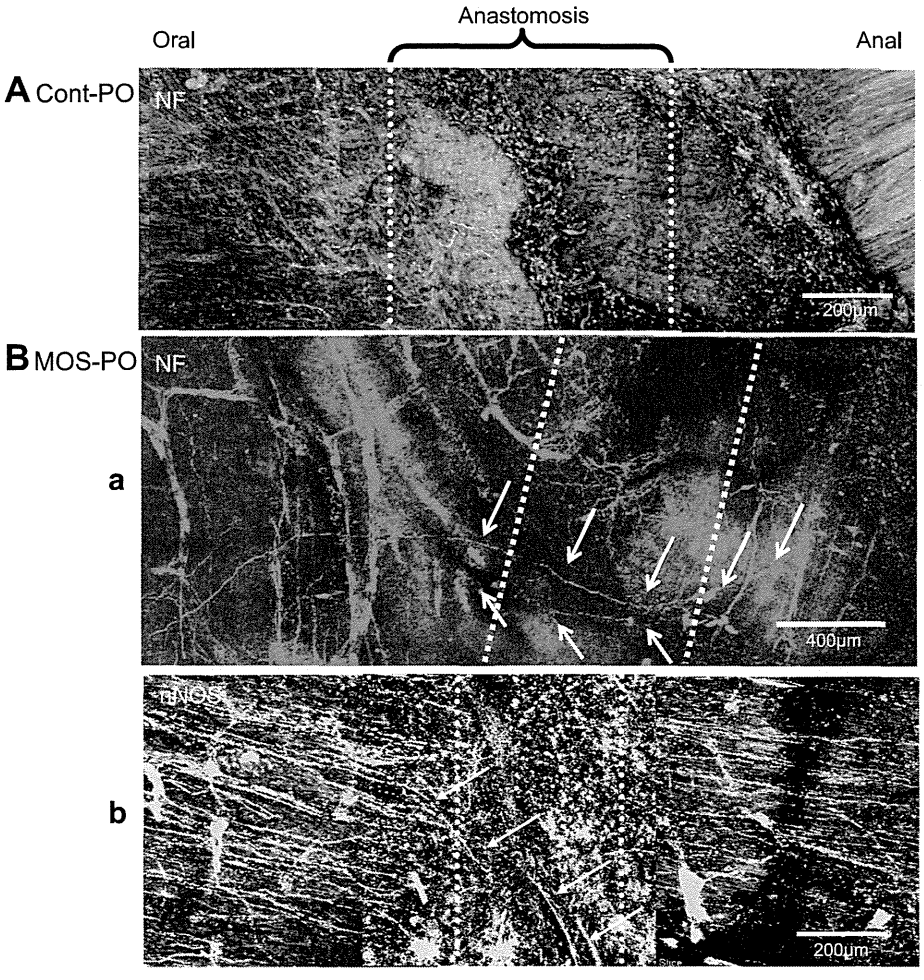

Fig. 6. Immunostaining for NF (red) and neuronal nitric oxide synthase (nNOS, green) in the rectal myenteric plexus 2 wk after RT+RA. *A*: 2 wk after vehicle in drinking water (Cont-PO), no bundles of fine nerve fibers can be seen between the oral and anal cut ends of the myenteric plexus. *B*: after MOS in drinking water (100 μmol/l; MOS-PO), numerous NF-positive bundles of fine nerve fibers can be seen between the oral and anal cut ends of the myenteric plexus as shown by arrows (*a*). Numerous nNOS-positive nerve fibers as shown by arrows are present at the anastomosis (*b*).